Supporting Information for

Formation of a Nickel Carbon Dioxide Adduct and its Transformation Mediated by a Lewis Acid

Yeong-Eun Kim, Jin Kim, Yunho Lee*

Department of Chemistry, Korea Advanced Institute of Science and Technology

Daejeon 305-701, Republic of Korea

Contents

Experimental Section.

EXPERIMENTAL SECTION

General Considerations. All manipulations were carried out using standard Schlenk or glovebox techniques under a N_2 atmosphere. Unless otherwise noted, solvents were deoxygenated and dried by thoroughly sparging with Ar gas followed by passage through an activated alumina column. Non-halogenated solvents were tested with a standard purple solution of sodium benzophenone ketyl in tetrahydrofuran in order to confirm effective oxygen and moisture removal. All reagents were purchased from commercial vendors and used without further purification unless otherwise stated. PPPCl[1] was prepared according to literature procedures. Elemental analyses were carried out at KAIST Central Research Instrument Facility on Thermo Scientific FLASH 2000 series instrument. Deuterated solvents were purchased from Cambridge Isotope Laboratories, Inc. or Euriso-top, degassed, and dried over activated 4 Å molecular sieves prior to use.

X-ray Crystallography. The diffraction data of **2**, **3** were collected on a Bruker SMART APEX II. The diffraction data of **4** were collected on a Bruker D8 QUEST. A suitable size and quality of crystal was coated with Paratone-*N* oil and mounted on a glass capillary. The data were collected with graphite-monochromated Mo Kα radiation (λ = 0.71073 Å) at 120 K. Cell parameters were determined and refined by SMART program.[2] Data reduction was performed using SAINT software.[3] An empirical absorption correction was applied using the SADABS program.[4]

Spectroscopic Measurements. Bruker 300 and 400 spectrometers were used to measure ¹H NMR. The chemical shifts for ¹H NMR spectra were quoted in part per million referenced to residual solvent peaks. The following abbreviations were used to describe peak splitting patterns when appropriate: s = singlet, d = doublet, t = triplet, q = quartet, m = multiplet, dd = doublet of doublet, dt = doublet of triplet, dq = doublet of quartet, br s = broad singlet. Coupling constants, *J*, were reported in hertz unit (Hz). ¹³C NMR spectra were recorded on Bruker 400 spectrometer. ¹³C NMR chemical shifts are reported in parts per million (ppm) referenced to internal solvent peaks. ³¹P NMR spectra were recorded on Bruker 400 and 600 spectrometers and were decoupled by broad band proton decoupling. The chemical shifts for ³¹P NMR spectra were quoted in part per million (ppm) referenced to external phosphoric acid as 0.0 ppm. ¹⁵N NMR spectra were recorded on Agilent 600 spectrometer and were decoupled by broad band proton

decoupling. The chemical shifts for ^{15}N NMR spectra were quoted in part per million (ppm) referenced to external formamide as –267.8 ppm. Electrospray ionization mass spectra (ESI-MS) were collected on a Bruker Daltonik (Germany) micrOTOF-Q II quadrupole ion trap instrument, by infusing samples directly into the source using a manual method. UV-vis spectra were measured by Agilent Cary 60 UV-Vis spectrophotometer using a 1 cm two-window quartz spectrophotometer cell sealed with a screw-cap purchased from Sigma-Aldrich Co. LLC. (Catalog number: Z276820). Infrared spectra were recorded in KBr pellet by Brucker VECTOR 33, Brucker EQUINOX 55 and Agilent 660-IR. Frequencies are given in reciprocal centimeters (cm^{-1}) and only selected absorbances were reported. Raman spectra were obtained on a Raman microscope equipped with a spectrometer (Acton Spectra Pro 2300i), a microscope (Olympus BX 43), and a thermoelectrically cooled 1024×127 pixel charge coupled device (CCD) detector (ANDOR, DV401A-BV). The 532 nm line of a continuous wave (CW) diode-pumped solid state (DPSS) laser (Cobolt, Samba) was used as an excitation source. A J-Young NMR tube with inner and outer diameters of 4.21 and 4.94 mm, respectively, was used for obtaining Raman spectra. The laser beam (20 mW) was focused inside the NMR tube with an objective lens ($\times 50$, NA = 0.55). The holographic grating (1200 grooves/mm) and the slit allowed the spectral resolution to be 2 cm^{-1}. The Raman bands of indene at 1018.3, 1205.6, and 1610.2 cm^{-1} were used to calibrate the spectrometer.

Computational details. Single-point calculation on **3** and $(dtbpe)Ni(\eta^2\text{-}CO_2)$ were run on the Gaussian09[5] with B3LYP density functional theory. Geometry for **3** was obtained from XRD data and that for $(dtbpe)Ni(\eta^2\text{-}CO_2)$ was obtained from the XRD data reported in literature.[6] Geometry optimization and NBO analysis for $(dtbpe)NiCOO\text{-}B(CH_3)_3$ and $(PP^{Me}P)NiCOOB(CH_3)_3$ were run on the Gaussian09[5] suite of programs with B3LYP level of theory. The lanl2dz basis set associated with effective core potential was used for describing a nickel atom and 6-31++G* basis set was used for all other atoms.

Synthesis of PP^MeP. To the cold suspension of PPPCl (2.299 g, 5.076 mmol) in 150 mL of diethyl ether was added MeMgCl (1.70 mL, 3.0 M in THF, 5.1 mmol) dropwise at –78 °C. The reaction mixture was warmed gradually to room temperature and stirred for additional 4 hr. The resulting solution was washed two times with the degassed water (100 mL). The separated organic layer was dried over anhydrous magnesium sulfate, and filtered through Ceilte. All volatiles were removed under vacuum. The product PP^MeP (1.990 g, 4.601 mmol, 90.63%) was isolated as a colorless oil after drying under vacuum. ^{1}H NMR (400 MHz, benzene-d_6, ppm) δ 7.32 (d, J = 7.20 Hz, 2H, Ar-H), 7.19 (s, 2H, Ar-H), 7.10 (t, J = 7.20 Hz, 2H, Ar-H), 7.05 (t, J = 7.20 Hz, 2H, Ar-H), 2.27 – 2.17 (m, 2H, CH), 2.01 (p, J = 7.00 Hz, 2H, CH), 1.68 (d, J = 5.60 Hz, 3H, P-CH$_3$), 1.27 – 1.11 (m, 12H, CHCH$_3$), 1.04 – 0.91 (m, 12H, CHCH$_3$). ^{13}C NMR (101 MHz, benzene-d_6, ppm) δ 150.16 (dd, J = 34.20, 5.20 Hz, C$_{Ar}$), 150.02 (dd, J = 33.20, 5.80 Hz, C$_{Ar}$), 141.70 (d, J = 18.00 Hz, C$_{Ar}$), 141.41 (d, J = 18.70 Hz, C$_{Ar}$), 131.76 (m, C$_{Ar}$), 131.68 (s, C$_{Ar}$), 24.57 (dd, J = 16.30, 5.20 Hz, CH$_{iPr}$), 24.18 (m, CH$_{iPr}$), 20.48 (d, J = 6.00 Hz, Me$_{iPr}$), 20.32 (d, J = 8.60 Hz, Me$_{iPr}$), 19.73 (d, J = 2.70 Hz, Me$_{iPr}$), 19.53 (d, J = 9.10 Hz, Me$_{iPr}$), 12.23 (dt, J = 19.20, 8.30 Hz, CH$_3$). ^{31}P NMR (162 MHz, benzene-d_6, ppm) δ –1.52 (d, J = 140.60 Hz), –35.34 (t, J = 140.90 Hz). ESI-MS {PP^MeP+H}$^+$: calcd, 433.23 ; found, 433.23.

Synthesis of {(PP^MeP)Ni}$_2$(μ-N$_2$) (2). After Ni(cod)$_2$ (0.277 g, 1.01 mmol) was added to the solution of PP^MeP (0.433 g, 1.00 mmol) in 50 mL of benzene in a 250 mL Schlenk tube, the reaction mixture was stirred for 5 hr at 90 °C. The resulting solution was filtered through Celite and volatiles were removed *in vacuo*. The product {(PP^MeP)Ni}$_2$(μ-N$_2$) (2, 0.358 g, 0.355 mmol, 70.9%) was isolated as a dark-brown solid after washing with pentane and drying under vacuum. Analytically pure compound was obtained from the recrystallization of the concentrated benzene solution of 2. The clean NMR spectra of 2 were obtained by degassing its C$_6$D$_6$ solution. ^{1}H NMR (400 MHz, benzene-d_6, ppm) δ 7.82 (s, 2H, Ar-H), 7.36 (s, 2H, Ar-H), 7.12 – 7.06 (m, 4H, Ar-H), 2.29 (s, 4H, -CH-), 1.98 (s, 3H, P-CH$_3$), 1.48 (s, 6H, CHCH$_3$), 1.36 (s, 6H, CHCH$_3$), 1.10 (s, 6H, CHCH$_3$), 0.82 (s, 6H, CHCH$_3$). ^{13}C NMR (101 MHz, benzene-d_6, ppm) δ 150.32 (dt, J = 30.60, 6.40 Hz, C$_{Ar}$), 146.91 (dt, J = 49.70, 14.60 Hz, C$_{Ar}$), 129.72 (s, C$_{Ar}$), 129.57 (s, C$_{Ar}$), 129.30 (t, J = 5.50 Hz, C$_{Ar}$), 128.59 (s, C$_{Ar}$), 30.22 (t, J = 9.20 Hz, CH$_{iPr}$), 25.49 (d, J = 18.80 Hz, CH$_{iPr}$), 20.89 (s, Me$_{iPr}$), 20.81 (s, Me$_{iPr}$), 20.28 (s, Me$_{iPr}$), 19.56 (s, Me$_{iPr}$), 16.14 (t, J = 11.40 Hz, P-CH$_3$). ^{31}P NMR (162 MHz, benzene-d_6, ppm) δ 64.75 (d, J = 68.85 Hz), 14.66 (t, J = 68.77 Hz). UV-Vis [benzene, nm (L mol^{-1} cm^{-1})]: 312 (21494), 387 (23277). IR (KBr pellet, cm^{-1}): v_{Ar}

5

= 1468. Raman (neat, cm^{-1}): $\nu_{N\equiv N}$ = 2045. Raman (benzene, cm^{-1}): $\nu_{N\equiv N}$ = 2042. Anal. Calcd. for {(PP^{Me}P)Ni}$_2$(μ-N$_2$): C, 59.44; H, 7.78; N, 2.77. Found: C, 59.53; H, 7.82; N, 2.40. Crystals suitable for X-ray diffraction were obtained by slow diffusion of pentane into a saturated benzene solution of **2**.

(PP^{Me}P)Ni(N$_2$) (1). The clean NMR spectra of **1** were obtained from its C$_6$D$_6$ solution (0.5 mM). ^{1}H NMR (400 MHz, benzene-d_6, ppm) δ 7.71 (s, 2H, Ar-H), 7.29 (s, 2H, Ar-H), 7.12 – 7.04 (m, 4H, Ar-H), 2.25 (s, 4H, -CH-), 1.83 (s, 3H, P-CH$_3$), 1.37 (s, 6H, CHCH$_3$), 1.19 (s, 6H, CHCH$_3$), 1.03 (s, 6H, CHCH$_3$), 0.79 (s, 6H, CHCH$_3$). ^{31}P NMR (162 MHz, benzene-d_6, ppm) δ 64.56 (d, J = 54.27 Hz), 19.02 (t, J = 54.19 Hz). Solution IR (KBr window, benzene, cm^{-1}): $\nu_{N\equiv N}$ = 2083.

(PP^{Me}P)Ni(^{15}N$_2$) (1-^{15}N$_2$) and {(PP^{Me}P)Ni}$_2$(μ-^{15}N$_2$) (2-^{15}N$_2$). In a NMR tube with a J-Young valve, **2** (0.011 g, 0.011 mmol) was dissolved in 0.5 mL benzene-d_6 or toluene-d_8. The solution was degassed by three freeze-pump-thaw cycles on the Schlenk line, and ^{15}N$_2$ gas was added at ambient pressure. The presence of both species (PP^{Me}P)Ni(^{15}N$_2$) (1-^{15}N$_2$) and {(PP^{Me}P)Ni}$_2$(μ-^{15}N$_2$) (2-^{15}N$_2$) at a ratio of 1:1 was confirmed by ^{1}H, ^{31}P, and ^{15}N NMR data. ^{15}N NMR (60 MHz, benzene-d_6, ppm) δ –70.4 (free ^{15}N$_2$), –73.1 (**1-^{15}N$_2$**, br s), –73.3 (**2-^{15}N$_2$**, s); (toluene-d_8, ppm) δ –53.7 (**1-^{15}N$_2$**, s), –70.4 (free ^{15}N$_2$), –71.3 (**1-^{15}N$_2$**, s), –74.9 (**2-^{15}N$_2$**, s). Solution IR (KBr window, benzene, cm^{-1}): $\nu_{N\equiv N}$ = 2013 for **1-^{15}N$_2$**. The clean NMR spectra of **2-^{15}N$_2$** were obtained by degassing its C$_6$D$_6$ solution. ^{15}N NMR (60 MHz, benzene-d_6, ppm) δ –73.3 (**2-^{15}N$_2$,** s); (toluene-d_8, ppm) δ –74.9 (**2-^{15}N$_2$,** s). Raman (benzene, cm^{-1}): $\nu_{N\equiv N}$ = 1974 for **2-^{15}N$_2$**.

Equilibrium studies. The concentrations of the two species involved in the equilibrium were determined by the integration of each methyl peak at 1.83 and 1.98 ppm which represents (PP^{Me}P)Ni(N$_2$) (**1**) and {(PP^{Me}P)Ni}$_2$(μ-N$_2$) (**2**), respectively. The concentration of N$_2$ (0.044 M) was obtained according to published methodology.[7] We used four different concentrations of compound **2** (6.19, 3.09, 1.54 and 0.77 mM) to obtain the equilibrium constant in this work; K$_{eq}$ = 8.6 ± 1.2 in benzene-d_6 at room temperature.

$$2\ (PP^{Me}P)Ni(N_2) \rightleftharpoons \{(PP^{Me}P)Ni\}_2(\mu\text{-}N_2) + N_2$$

$$K = \frac{[\{(PP^{Me}P)Ni\}_2(\mu\text{-}N_2)][N_2]}{[(PP^{Me}P)Ni(N_2)]^2} = 8.6 \pm 1.2 \text{ at RT}$$

Synthesis of (PP$^{\text{Me}}$P)N(η^2-CO$_2$) (3). In a 10 mL of Schlenk tube, the brown C$_6$H$_6$ solution of **2** (0.033 g, 0.032 mmol) was taken out of the dry-box and degassed by three freeze-pump-thaw cycles on the Schlenk line. After CO$_2$ gas was added at ambient pressure the dark brown solution was shaken causing an immediate color change to orange. The ^{1}H and ^{31}P NMR data reveal the formation of (PP$^{\text{Me}}$P)Ni(η^2-CO$_2$) (**3**, 0.032 g, 0.059 mmol, 92%) which was isolated as an orange powder. Analytically pure compound was obtained from the recrystallization of the concentrated benzene solution of **3** under CO$_2$ atmosphere. ^{1}H NMR (400 MHz, benzene-d_6, ppm) δ 7.63 (t, J = 6.50 Hz, 2H, Ar-H), 7.20 (d, J = 2.90 Hz, 2H, Ar-H), 7.05 (dt, J = 20.30, 7.40 Hz, 4H, Ar-H), 2.52 – 2.34 (m, 4H, CH), 1.70 – 1.58 (m, 6H, CH3, 3H, CH$_3$), 1.28 (dd, J = 6.50, 2.90 Hz, 6H, CH$_3$), 0.94 (dd, J = 5.00, 2.80 Hz, 6H, CH$_3$), 0.80 (dd, J = 6.40, 2.80 Hz, 6H, CH$_3$). ^{31}P NMR (162 MHz, benzene-d_6, ppm) δ 57.58 (d, J = 5.99 Hz), 47.64 (t, J = 6.32 Hz). UV-Vis [benzene, nm (L mol^{-1} cm^{-1})]: 421 (3126.2). IR (KBr pellet, cm^{-1}): $\nu_{\text{C=O}}$ = 1682, 1629. Anal. Calcd. for (PP$^{\text{Me}}$P)Ni(CO$_2$): C, 58.35; H, 7.34; N, 0.00. Found: C, 58.19; H, 7.33; N, 0.00. Crystals suitable for X-ray diffraction were obtained by cooling down of saturated benzene solution of **3**.

(PP$^{\text{Me}}$P)Ni(η^2-^{13}CO$_2$) (3-^{13}CO$_2$). In a NMR tube with a J-Young valve, the brown C$_6$D$_6$ solution of **2** (0.008 g, 0.008 mmol) was taken out of the dry-box and degassed by three freeze-pump-thaw cycles on the Schlenk line. After ^{13}CO$_2$ gas was added at ambient pressure the dark brown solution was shaken causing an immediate color change to orange. Spectroscopic features in the ^{1}H NMR spectrum were identical for **3**. ^{13}C NMR (101 MHz, benzene-d_6, ppm) δ 164.70 (d, J_{PC} = 51.40 Hz), 124.75 (s, free ^{13}CO$_2$). ^{31}P NMR (162 MHz, benzene-d_6, ppm) δ 57.54 (d, J = 5.90 Hz), 47.70 (dt, J = 51.70, 5.60 Hz). IR (KBr pellet, cm^{-1}): $\nu_{\text{C=O}}$ = 1638, 1585.

Synthesis of (PP$^{\text{Me}}$P)Ni{COOB(C$_6$F$_5$)$_3$} (4). In a 100 mL Schlenk tube, the brown solution of **2** (0.059 g, 0.058 mmol) in THF (30 mL) was degassed by three freeze-pump-thaw cycles on the Schlenk line. After CO$_2$ gas was added at ambient pressure the dark brown solution was stirred causing an immediate color change to orange. To a frozen mixture was added B(C$_6$F$_5$)$_3$ (0.060 g, 0.12 mmol) in 5 mL THF under Ar. The reaction mixture was slowly warmed to room temperature and stirred for additional 5 hr. All volatiles were removed *in vacuo*, and the resulting product (PP$^{\text{Me}}$P)Ni{COOB(C$_6$F$_5$)$_3$} (**4**, 0.078 g, 0.075 mmol, 64%) was isolated as a yellow solid after washing with pentane and drying under vacuum. ^{1}H NMR (400 MHz, benzene-d_6, ppm) δ 7.35 (t, J = 6.60 Hz, 2H, Ar-H), 7.23 – 7.10 (m, 2H, Ar-H), 7.01 – 6.89 (m, 4H, Ar-H), 2.50 (q, J

= 7.20 Hz, 2H, CH), 2.29 (s, 2H, CH), 1.35 (d, J = 7.50 Hz, 3H, CH$_3$), 1.29 (dd, J = 16.80, 7.20 Hz, 6H, CH$_3$), 0.89 (dd, J = 17.40, 7.40 Hz, 6H, CH$_3$), 0.83 – 0.74 (m, 12H, CH$_3$). ^{31}P NMR (162 MHz, benzene-d_6, ppm) δ 64.07 (t, J = 20.60 Hz), 63.56 (d, J = 20.30 Hz). UV-Vis [benzene, nm (L mol^{-1} cm^{-1})]: 309 (7115), 439 (1753). IR (KBr pellet, cm^{-1}): ν_{CO} = 1631 (sh), 1277. Anal. Calcd. for (PP^{Me}P)Ni(COOB(C$_6$F$_5$)$_3$): C, 50.47; H, 3.75; N, 0.00. Found: C, 50.23; H, 3.74; N, 0.00. Crystals suitable for X-ray diffraction were obtained by slow diffusion of pentane into a saturated toluene solution of **4**.

(PP^{Me}P)Ni{^{13}COOB(C$_6$F$_5$)$_3$} (4-^{13}CO$_2$). In a 25 mL Schlenk tube, the brown solution of **2** (0.019 g, 0.019 mmol) in 10 mL THF was degassed by three freeze-pump-thaw cycles on the Schlenk line. After CO$_2$ gas was added at ambient pressure the dark brown solution was stirred causing an immediate color change to orange. To a frozen mixture was added B(C$_6$F$_5$)$_3$ (0.020 g, 0.038 mmol) in 5 mL THF under Ar. The reaction mixture was slowly warmed to room temperature and stirred for 5 hr. Volatiles were removed *in vacuo* and the resulting product (PP^{Me}P)Ni{^{13}COOB(C$_6$F$_5$)$_3$} (**4-^{13}CO$_2$**, 0.021 g, 0.020 mmol, 53%) was isolated as a yellow solid after washing with pentane and drying under vacuum. Spectroscopic features in the ^{1}H NMR spectrum were identical for **4**. ^{13}C NMR (101 MHz, benzene-d_6, ppm) δ 185.47 (dt, J_{PC} = 104.20, 14.04 Hz). ^{31}P NMR (243 MHz, benzene-d_6, ppm) δ 64.11 (d, J = 103.99 Hz), 63.49 (dd, J = 19.90, 14.10 Hz). IR (KBr pellet, cm^{-1}): ν_{CO} = 1604, 1261.
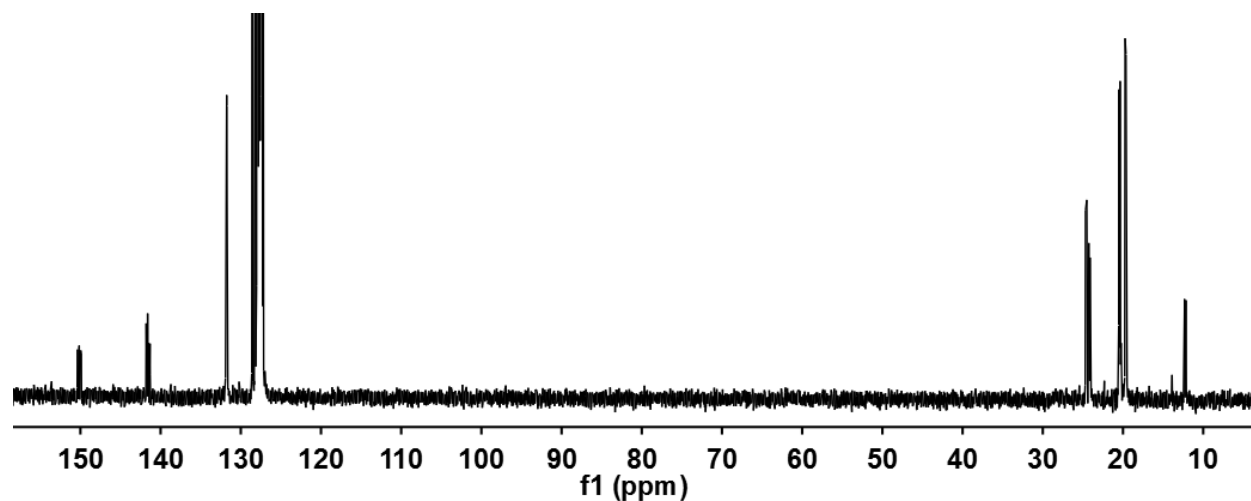
Figure S1. ^{1}H NMR spectrum of PP^{Me}P in benzene-d_6 at room temperature.
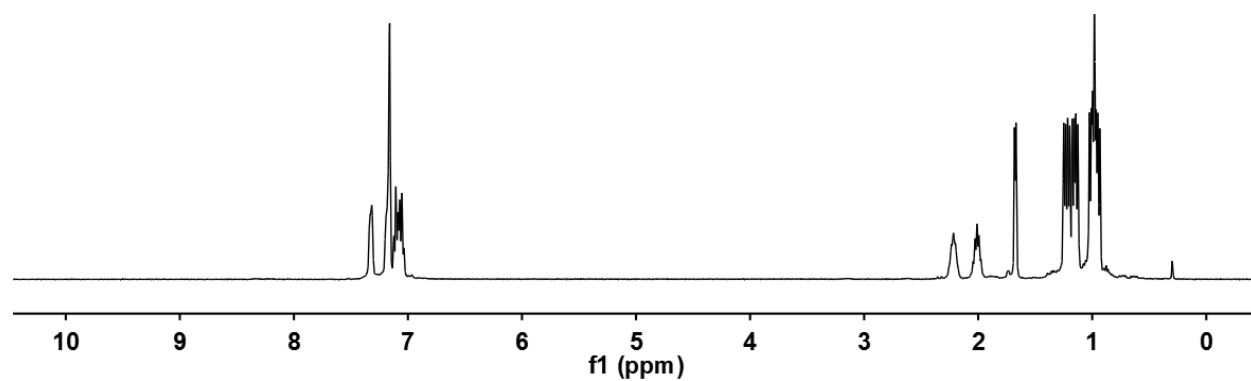
Figure S2. ^{31}P NMR spectrum of PP^{Me}P in benzene-d_6 at room temperature.
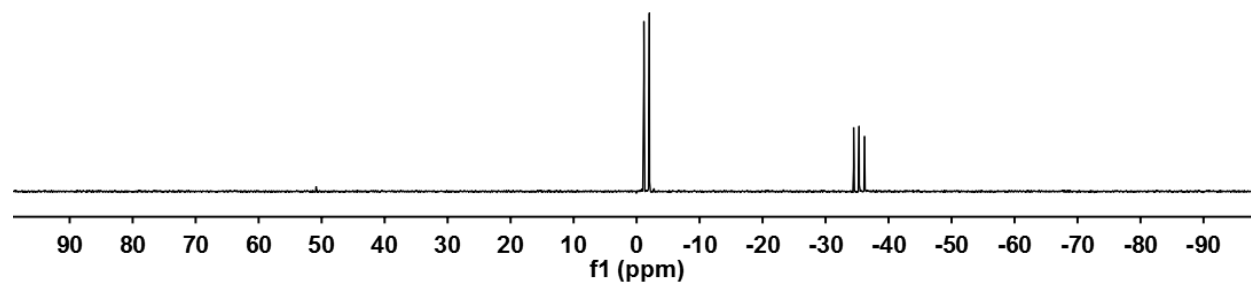
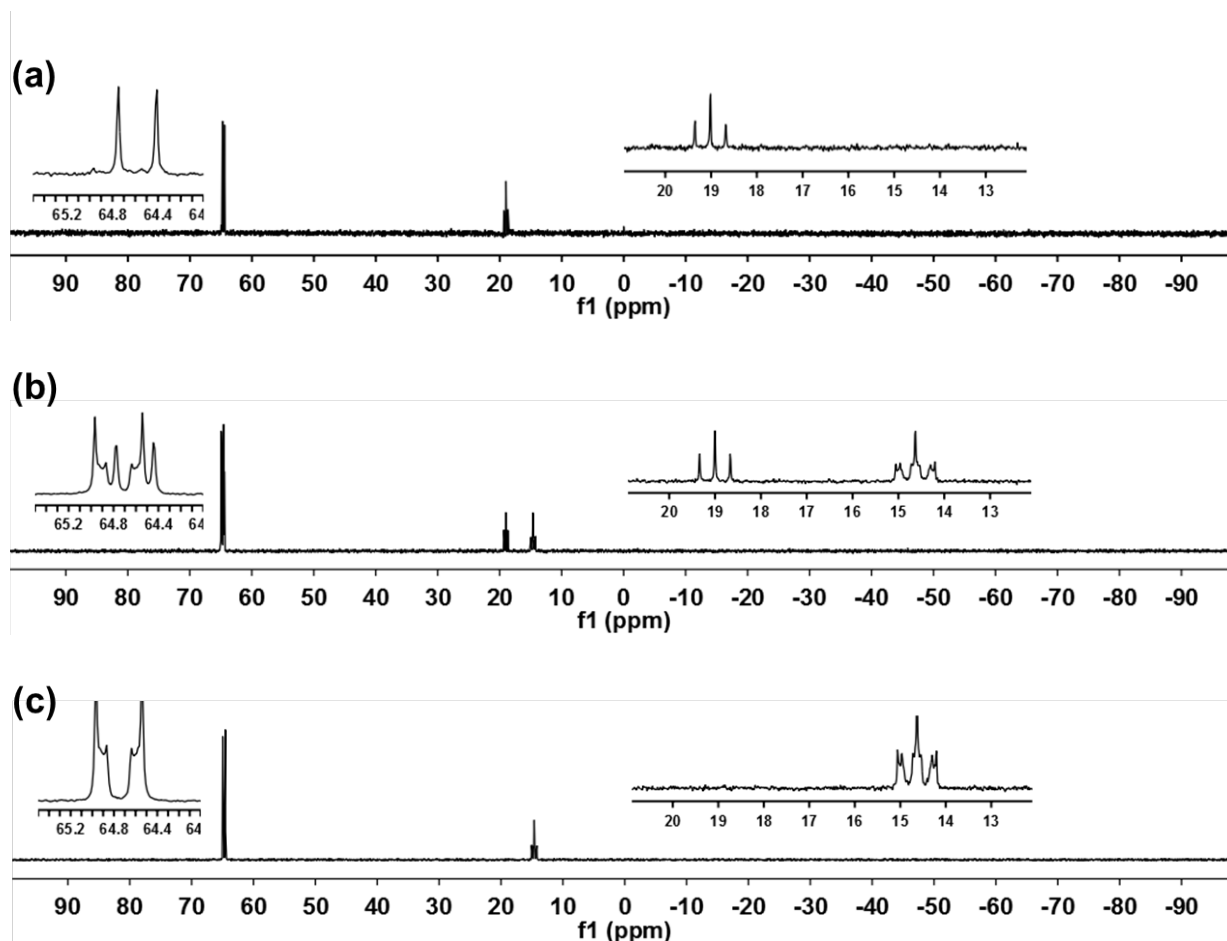**Figure S3.** ^{13}C NMR spectrum of PP^{Me}P in benzene-d_6 at room temperature.

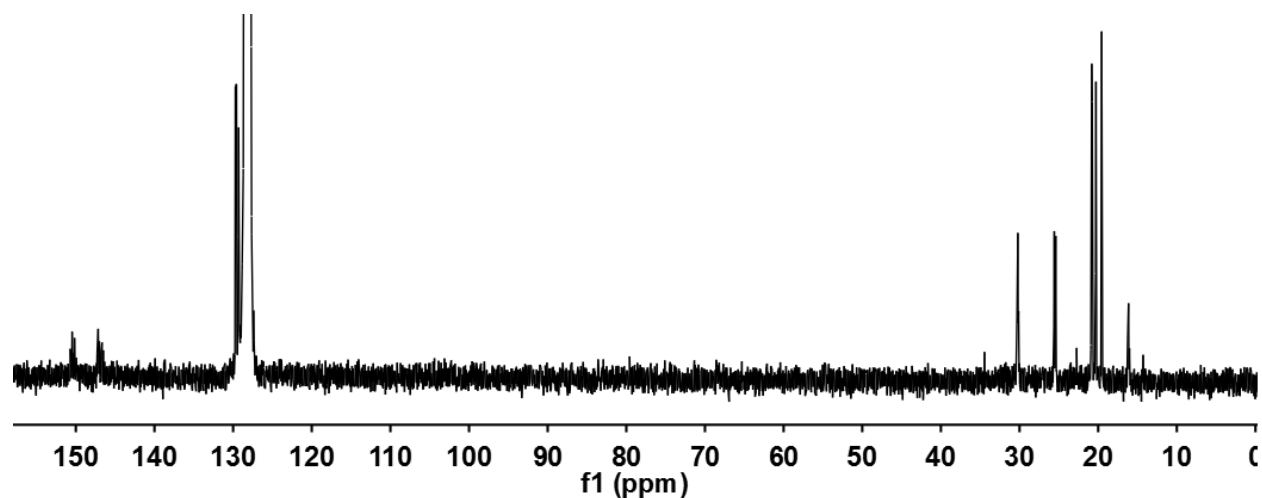**Figure S4.** ^{1}H NMR spectra of (a) (PP^{Me}P)Ni(N$_2$) (**1**), (b) (PP^{Me}P)Ni(N$_2$) (**1**) and {(PP^{Me}P)Ni}$_2$(μ-N$_2$) (**2**) under N$_2$ atmosphere (1 atm) and (c) {(PP^{Me}P)Ni}$_2$(μ-N$_2$) (**2**) under vacuum in benzene-d_6 at room temperature.
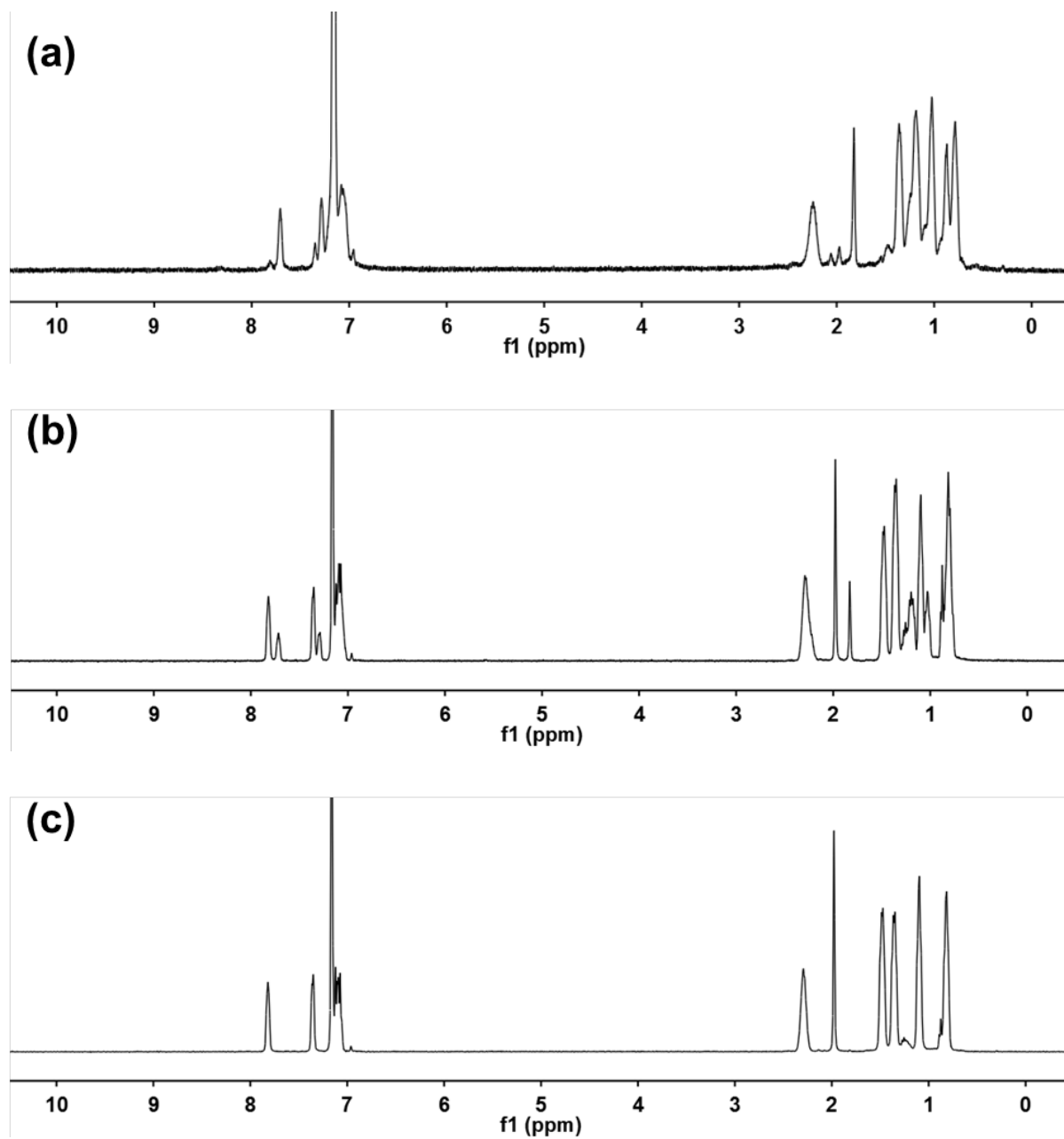
Figure S5. ^{31}P NMR spectra of (a) (PP^{Me}P)Ni(N$_2$) (**1**), (b) (PP^{Me}P)Ni(N$_2$) (**1**) and {(PP^{Me}P)Ni}$_2$(μ-N$_2$) (**2**) under N$_2$ atmosphere (1 atm) and (c) {(PP^{Me}P)Ni}$_2$(μ-N$_2$) (**2**) under vacuum in benzene-d_6 at room temperature.

Figure S6. ^{13}C NMR spectrum of {(PP^{Me}P)Ni}$_2$(μ-N$_2$) (**2**) under vacuum in benzene-d_6 at room temperature.

Figure S7. ^{15}N NMR spectra of (a) a mixture of $(PP^{Me}P)Ni(N_2)$ (**1**) and $\{(PP^{Me}P)Ni\}_2(\mu\text{-}N_2)$ (**2**) under $^{15}N_2$ atmosphere (1 atm), and (b) $\{(PP^{Me}P)Ni\}_2(\mu\text{-}N_2)$ (**2**) under vacuum in benzene-d_6 at room temperature.
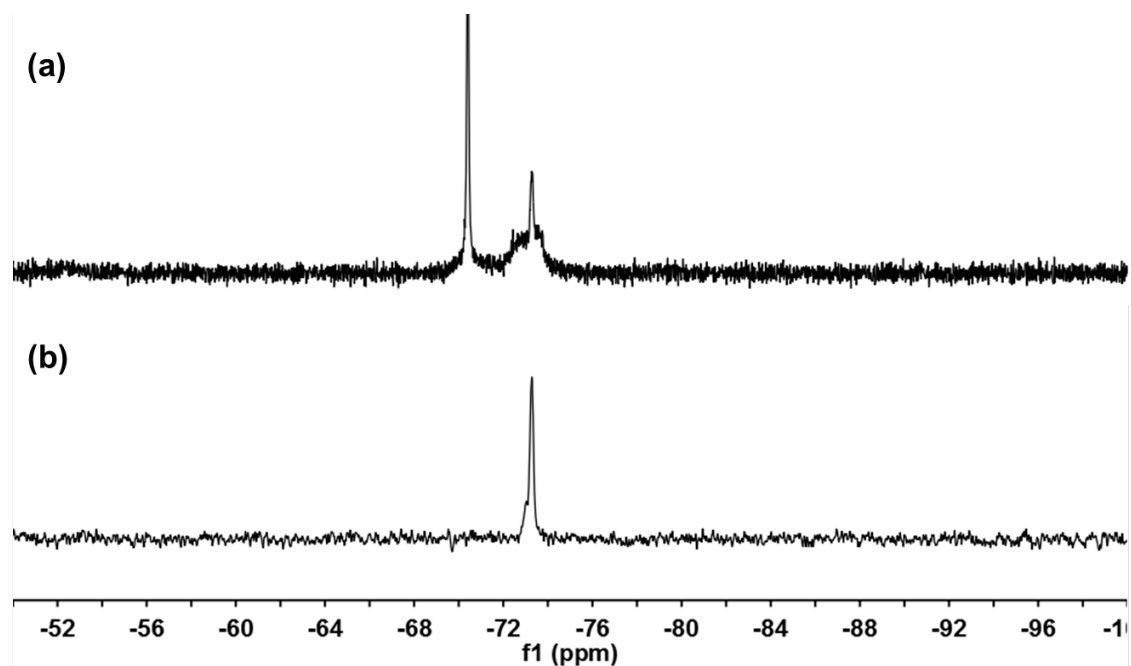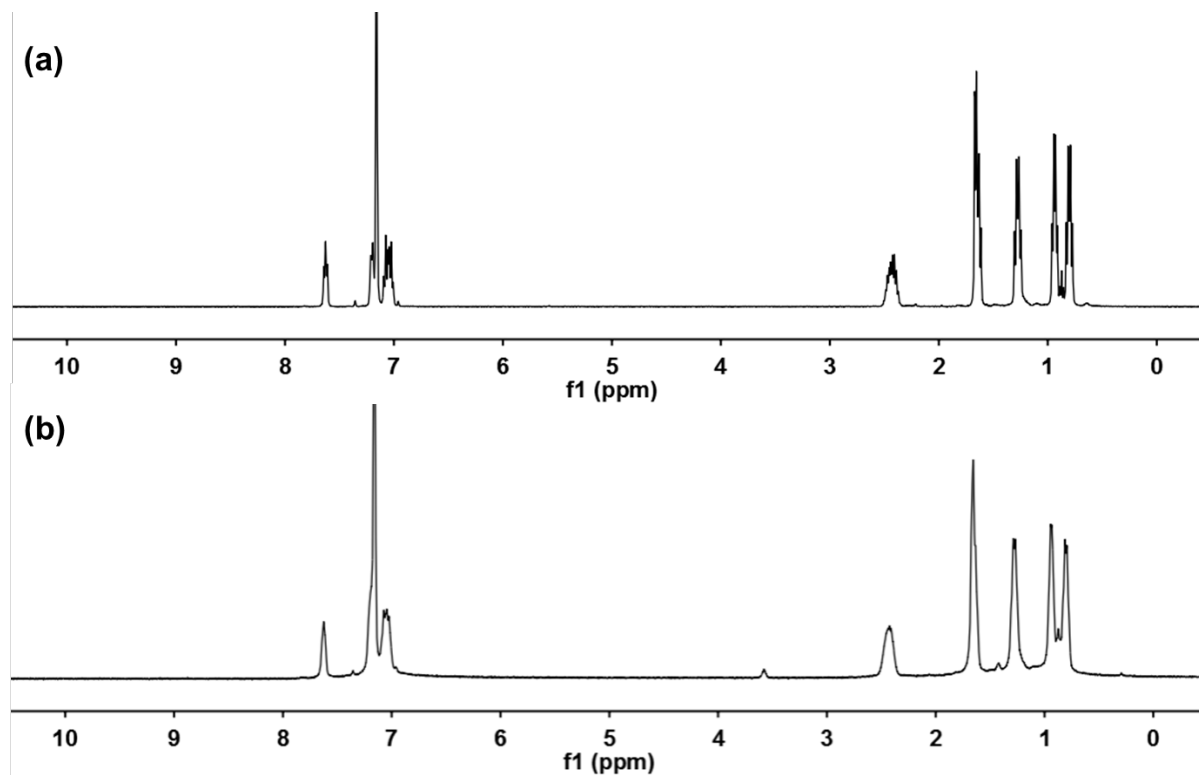

Figure S8. ^{15}N NMR spectra of (a) a mixture of $(PP^{Me}P)Ni(N_2)$ (**1**) and $\{(PP^{Me}P)Ni\}_2(\mu\text{-}N_2)$ (**2**) under $^{15}N_2$ atmosphere (1 atm), and (b) $\{(PP^{Me}P)Ni\}_2(\mu\text{-}N_2)$ (**2**) under vacuum in toluene-d_8 at $-60\ ^\circ C$.
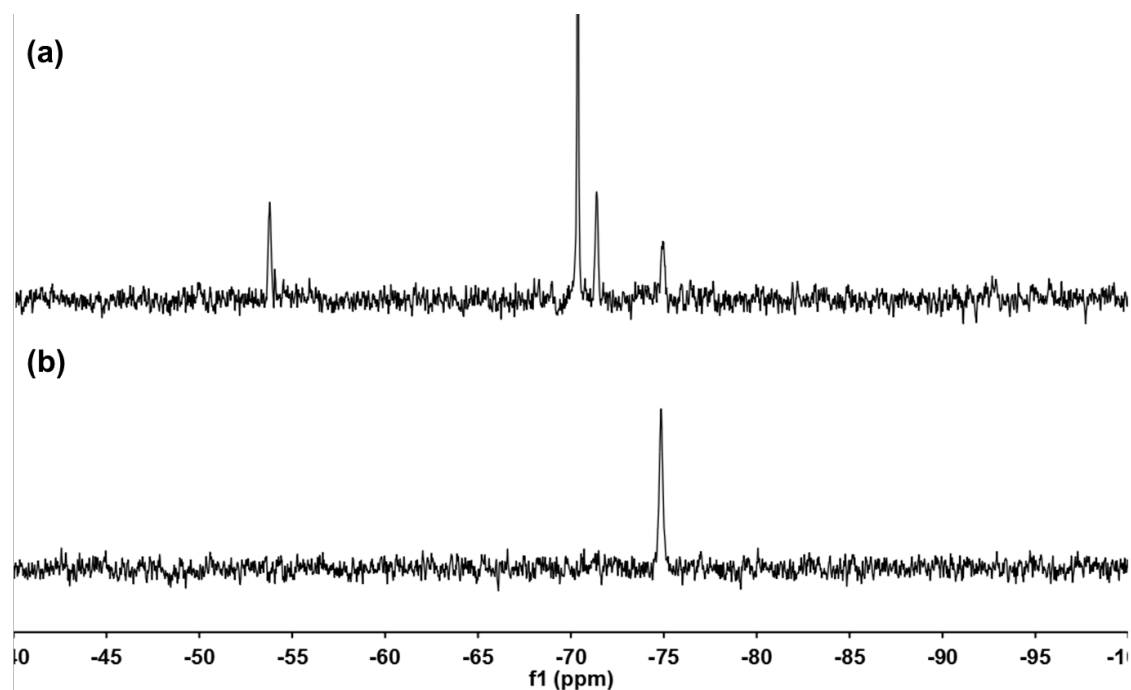
Figure S9. ^{1}H NMR spectrum of $(PP^{Me}P)Ni(\eta^2\text{-}CO_2)$ (**3**) under (a) CO_2 atmosphere and (b) vacuum in benzene-d_6 at room temperature.

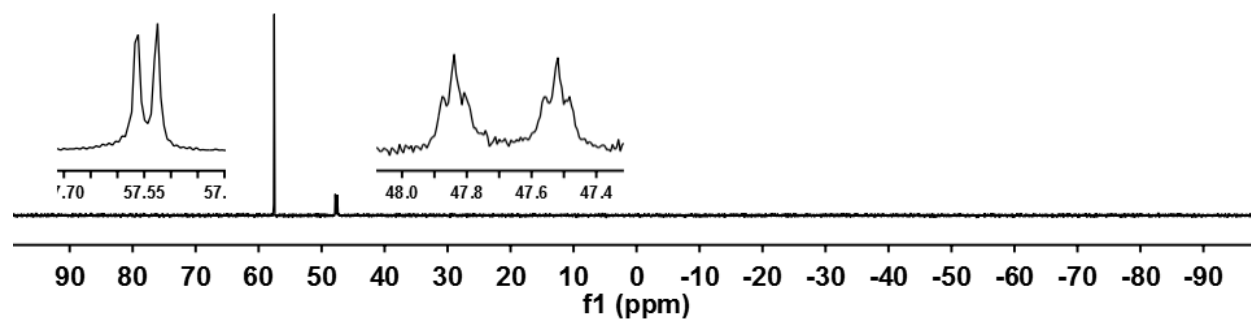**Figure S10.** ^{31}P NMR spectrum of $(PP^{Me}P)Ni(\eta^2\text{-}CO_2)$ (**3**) under (a) CO_2 atmosphere and (b) vacuum in benzene-d_6 at room temperature.
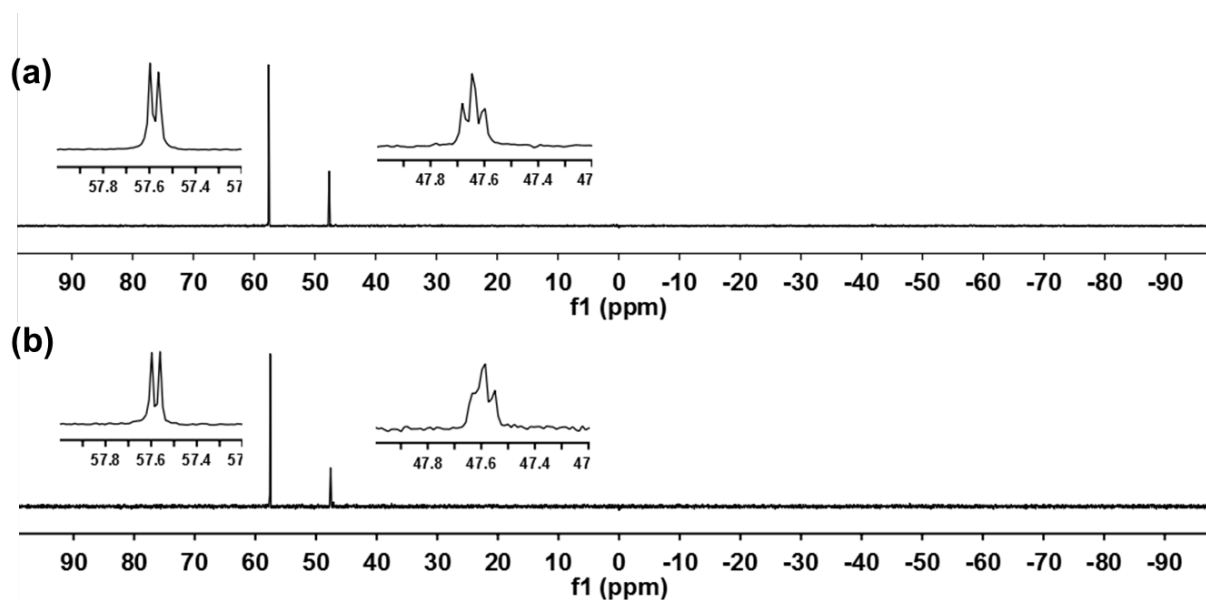
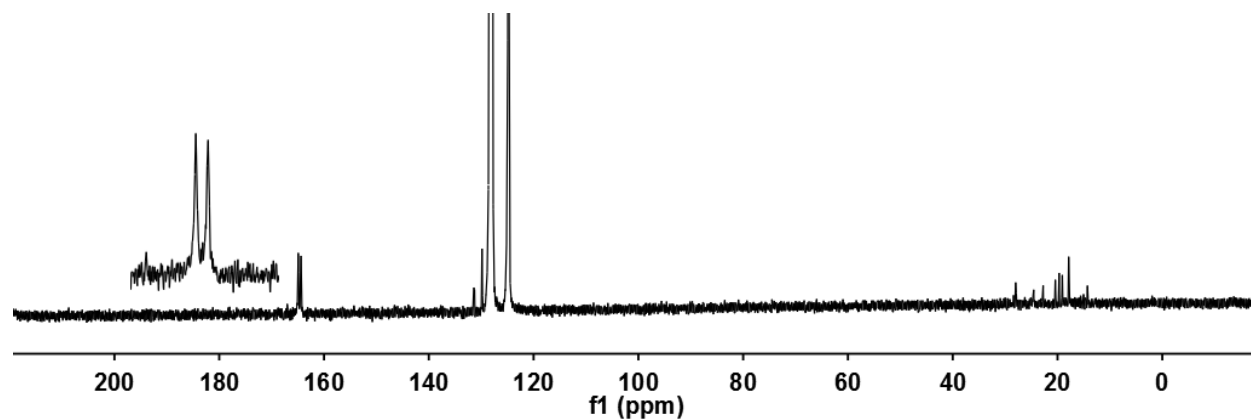**Figure S11.** ^{1}H NMR spectrum of $(PP^{Me}P)Ni(\eta^2\text{-}^{13}CO_2)$ (**3-$^{13}CO_2$**) in benzene-d_6 at room temperature.
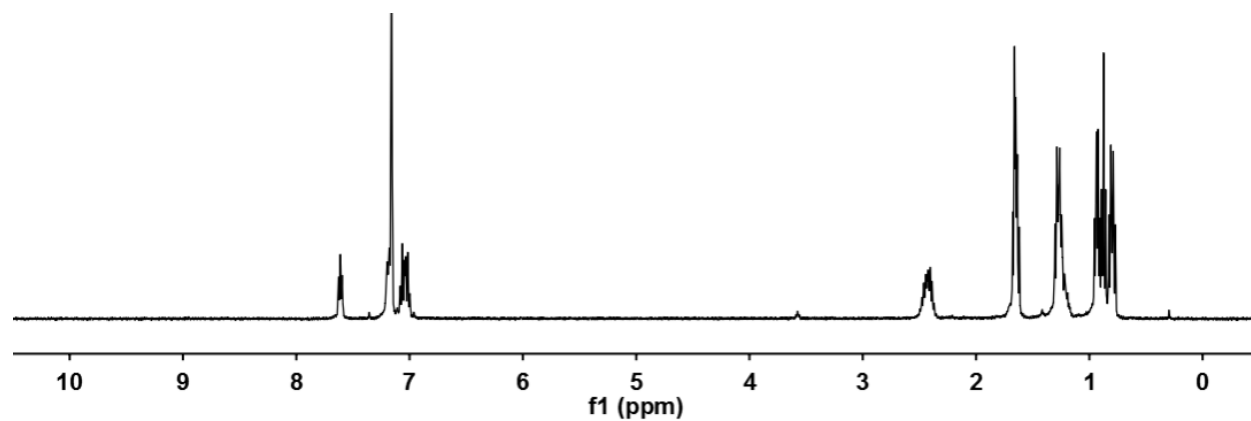
Figure S12. ^{31}P NMR spectrum of $(PP^{Me}P)Ni(\eta^2\text{-}^{13}CO_2)$ (**3-$^{13}CO_2$**) in benzene-d_6 at room temperature.

Figure S13. ^{13}C NMR spectrum of $(PP^{Me}P)Ni(\eta^2\text{-}^{13}CO_2)$ (**3-$^{13}CO_2$**) in benzene-d_6 at room temperature.

14

Figure S14. ^{1}H NMR spectrum of (PP^{Me}P)Ni{COOB(C$_6$F$_5$)$_3$} (**4**) in benzene-d_6 at room temperature.
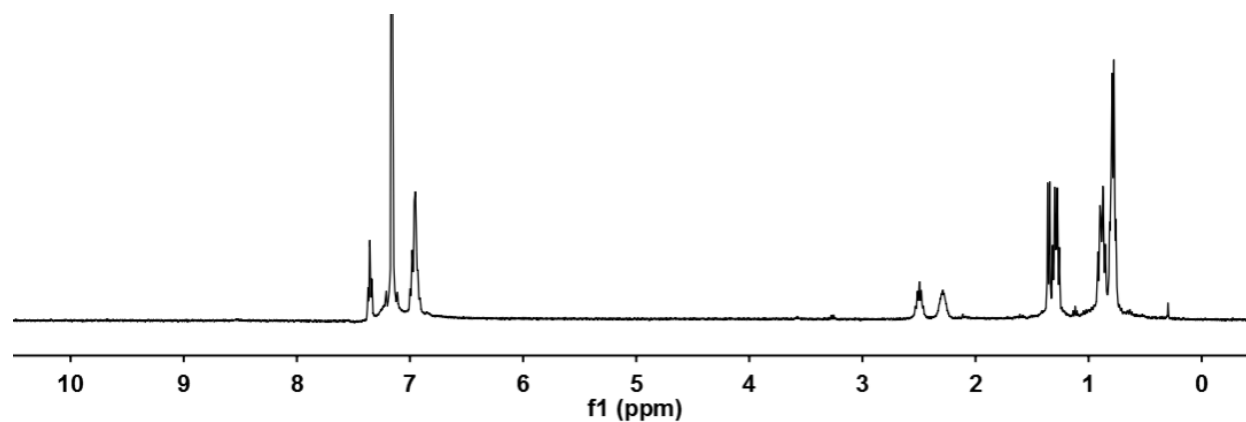
Figure S15. ^{31}P NMR spectrum of (PP^{Me}P)Ni{COOB(C$_6$F$_5$)$_3$} (**4**) in benzene-d_6 at room temperature.
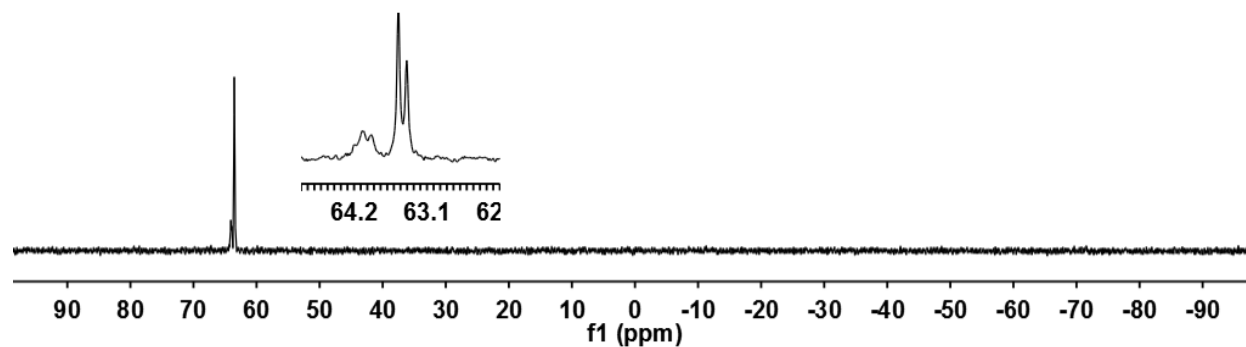
Figure S16. ^1H NMR spectrum of $(PP^{Me}P)Ni\{^{13}COOB(C_6F_5)_3\}$ (**4-$^{13}CO_2$**) in benzene-d_6 at room temperature.
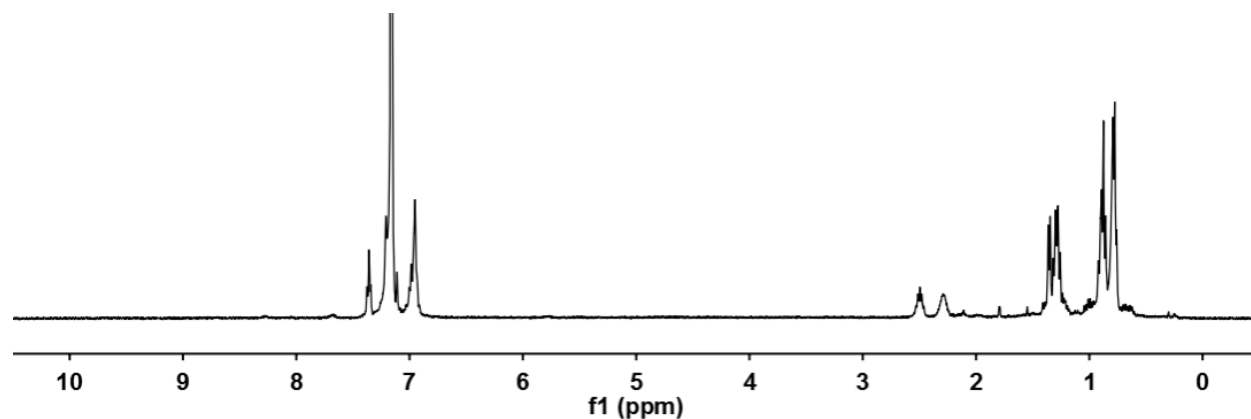
Figure S17. ^{31}P NMR spectrum of $(PP^{Me}P)Ni\{^{13}COOB(C_6F_5)_3\}$ (**4-$^{13}CO_2$**) in benzene-d_6 at room temperature.
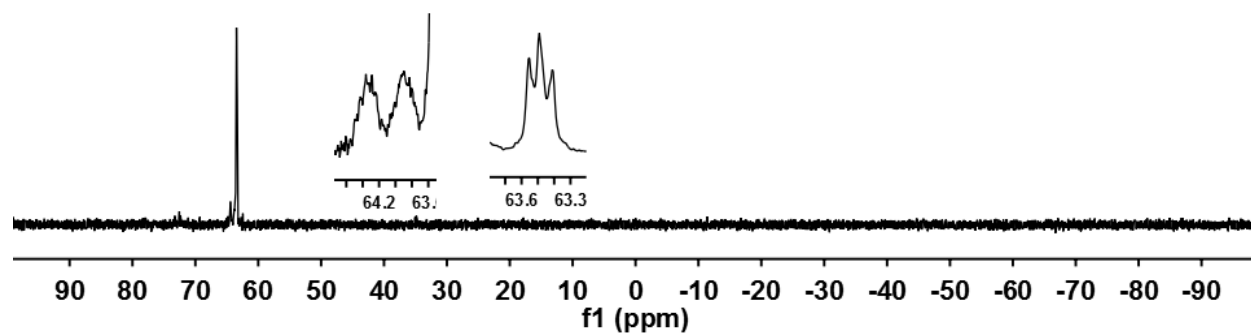
Figure S18. Experimental (black) and simulated (red) ^{31}P NMR spectra of $(PP^{Me}P)Ni\{^{13}COO-B(C_6F_5)_3\}$ (**4-$^{13}CO_2$**).

Simulation parameter:
Spin = 1/2
Line width = 10 Hz
J = 19.9, 14.1 Hz

16
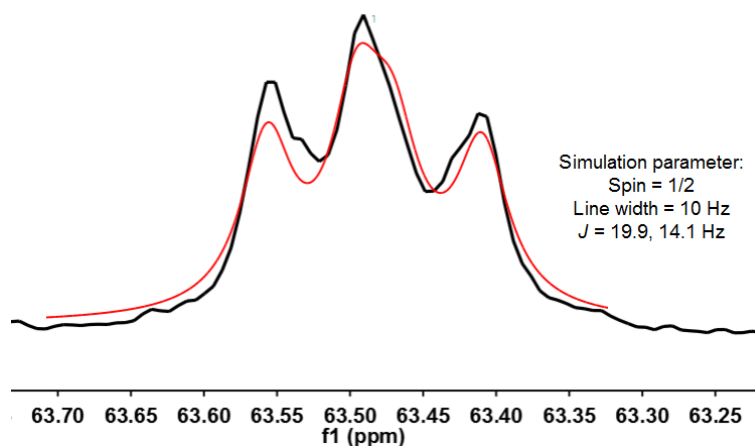
Figure S19. ^{13}C NMR spectrum of $(PP^{Me}P)Ni\{^{13}COOB(C_6F_5)_3\}$ **(4-$^{13}CO_2$)** in benzene-d_6 at room temperature.
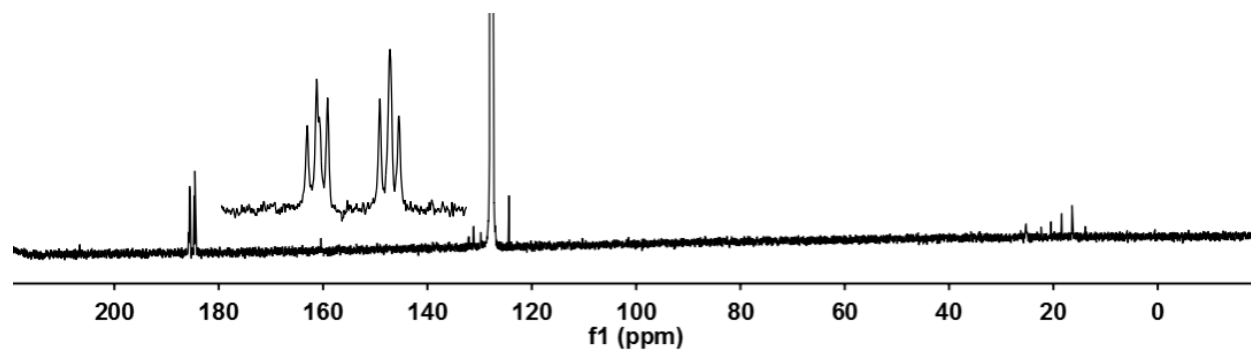
**Figure S20.** Solid-state structure of $\{(PP^{Me}P)Ni\}_2(\mu\text{-}N_2)$ (**2**). Hydrogen atoms are omitted for clarity.
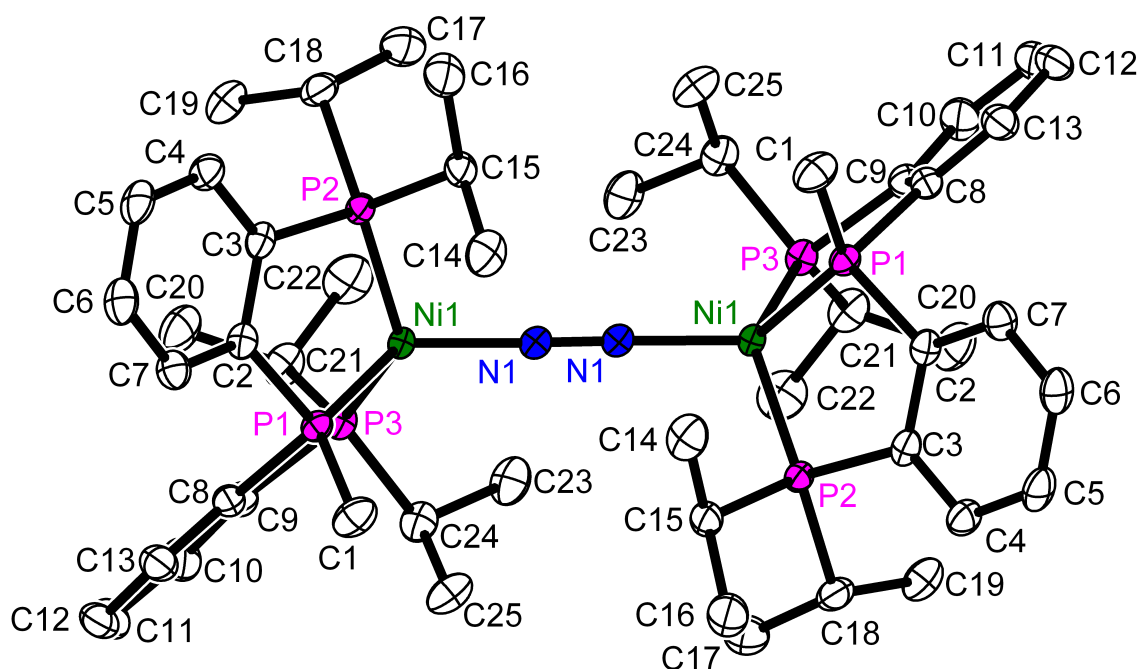
Table S1. Selected bond distances and angles for $\{(PP^{Me}P)Ni\}_2(\mu\text{-}N_2)$ (**2**) (Å and °).

| Distance	**2**	Angle	**2**
d_{N1-N1}	1.124(3)	$\angle$Ni1-N1-N1	178.6(2)
d_{Ni1-N1}	1.830(2)	$\angle$P1-Ni1-N1	124.72(5)
d_{Ni1-P1}	2.1168(5)	$\angle$P2-Ni1-N1 $\angle$P3-Ni1-N1	105.91(5) 110.92(5)
d_{Ni1-P2}	2.1627(5)	$\angle$P1-Ni1-P2 $\angle$P1-Ni1-P3	90.72(2) 91.47(2)
d_{Ni1-P3}	2.1544(5)	$\angle$P2-Ni1-P3	133.05(2)

Figure S21. Solid-state structure of $(PP^{Me}P)Ni(\eta^2\text{-}CO_2)$ (**3**). Hydrogen atoms are omitted for clarity.
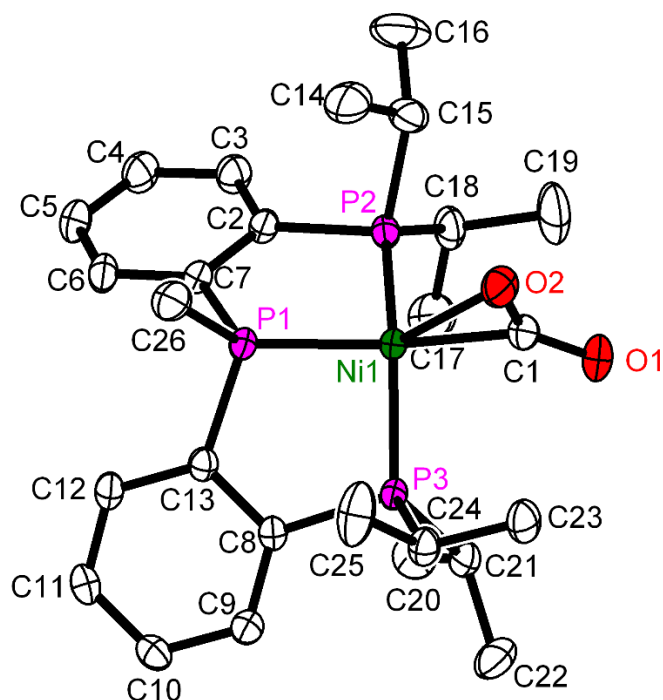
Table S2. Selected bond distances and angles for $(PP^{Me}P)Ni(\eta^2\text{-}CO_2)$ (**3**) (Å and °).

Distance	**3**	Angle	**3**
$d_{Ni1\text{-}C1}$	1.904(1)	∠P1-Ni1-P2 ∠P1-Ni1-P3	89.19(1) 90.03(1)
$d_{Ni1\text{-}O2}$	2.191(1)	∠P2-Ni1-P3	143.03(2)
$d_{C1\text{-}O1}$ $d_{C1\text{-}O2}$	1.218(2) 1.252(2)	∠O1-C1-O2 ∠Ni1-C1-O1 ∠Ni1-C1-O2	135.1(1) 139.5(1) 85.30(9)
$d_{Ni1\text{-}P1}$	2.1631(4)	∠C1-Ni1-P1	165.89(5)
$d_{Ni1\text{-}P2}$ $d_{Ni1\text{-}P3}$	2.1860(4) 2.1633(4)	∠C1-Ni1-P2 ∠C1-Ni1-P3	95.76(5) 93.85(5)

Figure S22. Solid-state structure of $(PP^{Me}P)Ni\{COOB(C_6F_5)_3\}$ (**4**). A co-crystallized toluene solvent molecule and hydrogen atoms are omitted for clarity.
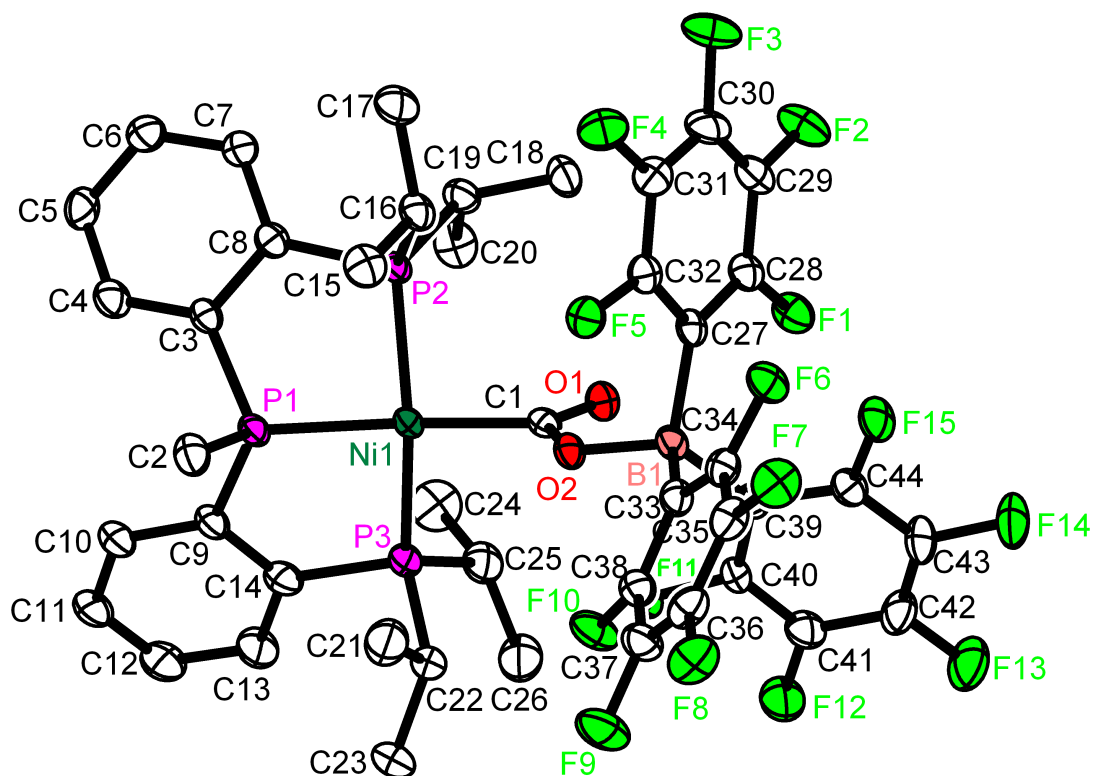

Table S3. Selected bond distances and angles for $(PP^{Me}P)Ni\{COOB(C_6F_5)_3\}$ (**4**) (Å and °).

Distance	**4**	Angle	**4**
d_{Ni1-C1}	1.923(3)	∠P1-Ni1-P2 ∠P1-Ni1-P3	87.99(4) 87.90(4)
d_{C1-O1} d_{C1-O2}	1.223(4) 1.340(4)	∠P2-Ni1-P3	154.43(4)
d_{B1-O2}	1.532(4)	∠O1-C1-O2 ∠Ni1-C1-O1 ∠Ni1-C1-O2	122.9(3) 129.7(3) 107.4(2)
d_{Ni1-P1}	2.179(1)	∠C1-Ni1-P1	173.8(1)
d_{Ni1-P2} d_{Ni1-P3}	2.167(1) 2.183(1)	∠C1-Ni1-P2 ∠C1-Ni1-P3	133.18(5) 133.20(4)

Figure S23. UV-Vis spectra of a mixture of $(PP^{Me}P)Ni(N_2)$ (**1**) and $\{(PP^{Me}P)Ni\}_2(\mu\text{-}N_2)$ (**2**) under N_2 atmosphere (1 atm) (red) and $\{(PP^{Me}P)Ni\}_2(\mu\text{-}N_2)$ (**2**) under vacuum (blue) in benzene at room temperature.
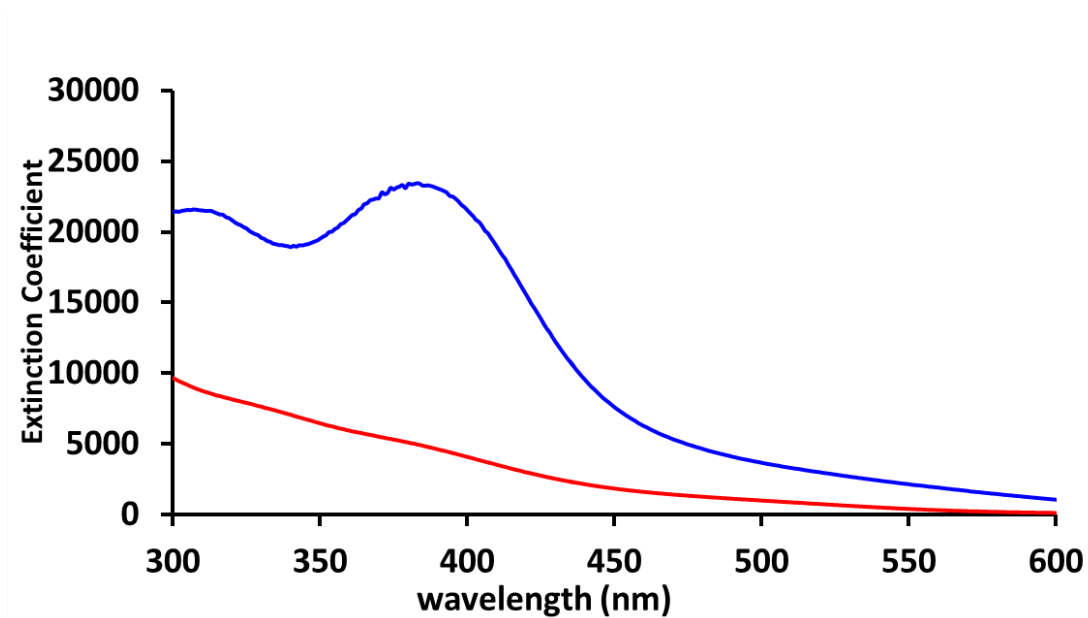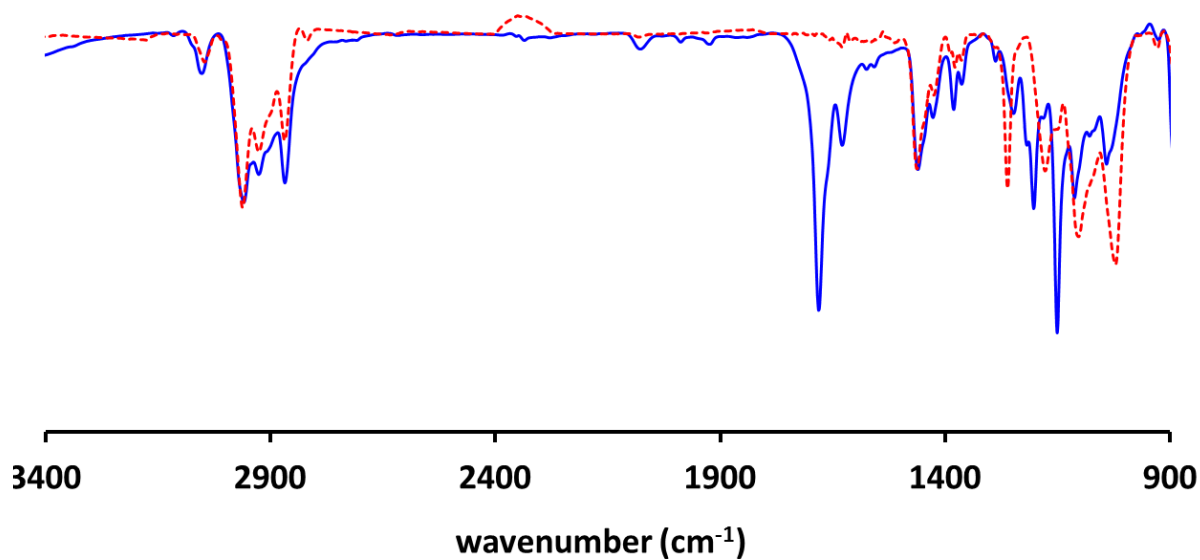

Figure S24. UV-Vis spectra of $(PP^{Me}P)Ni(\eta^2\text{-}CO_2)$ (**3**, red) $(PP^{Me}P)Ni\{COOB(C_6F_5)_3\}$ (**4**, blue) in benzene at room temperature.
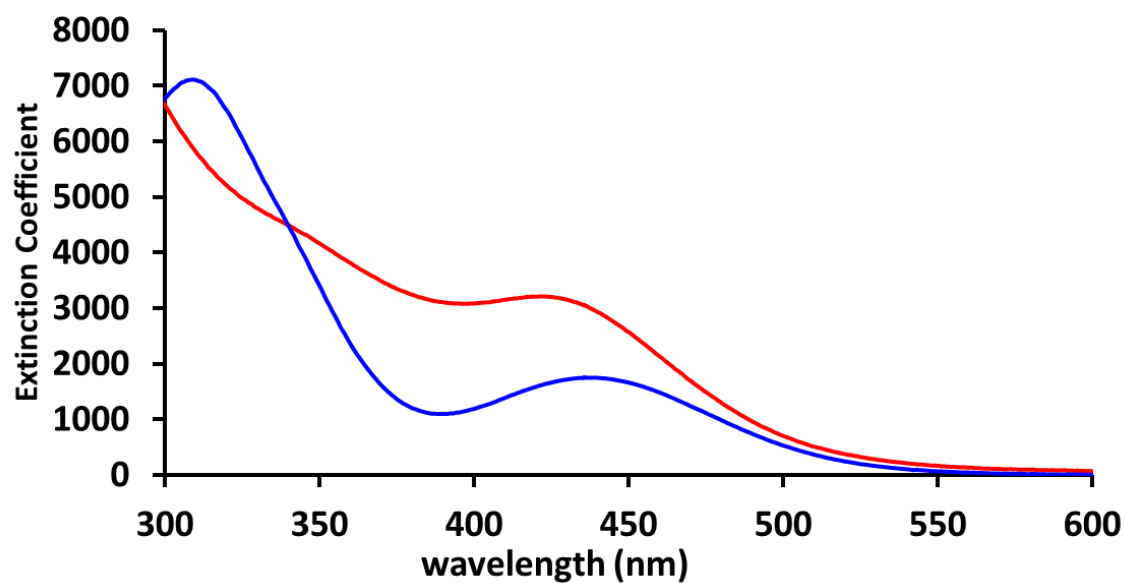
Figure S25. IR spectra of PP^{Me}P (dotted red line) and $\{(PP^{Me}P)Ni\}_2(\mu\text{-}N_2)$ (**2**, blue line) (KBr pellet).
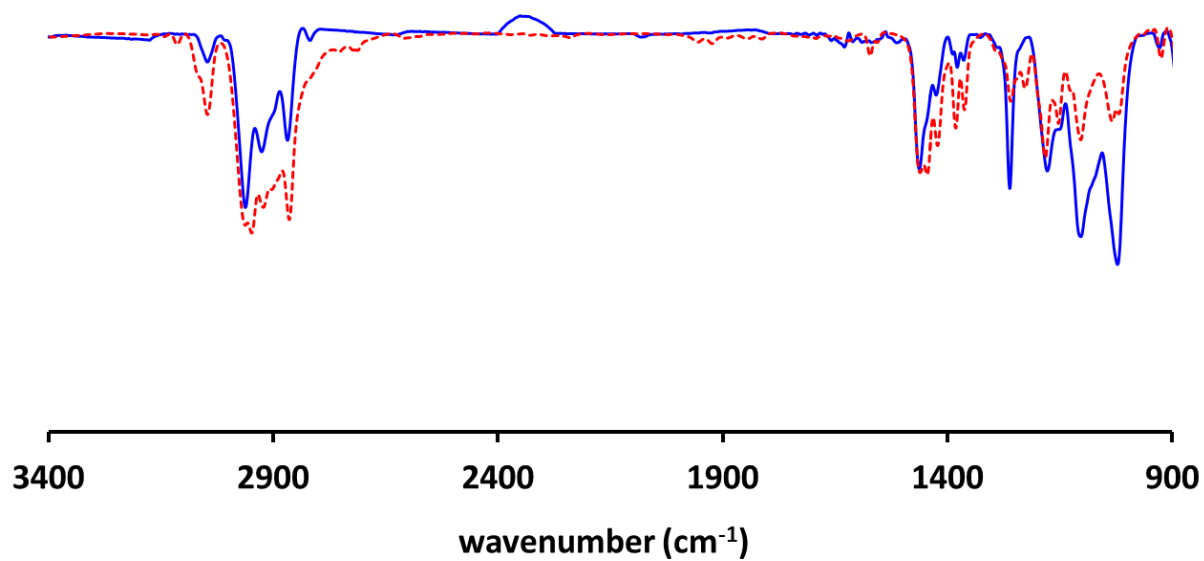
Figure S26. IR spectra of $\{(PP^{Me}P)Ni\}_2(\mu\text{-}N_2)$ (**2**, dotted red line) and $(PP^{Me}P)Ni(\eta^2\text{-}CO_2)$ (**3**, blue line) (KBr pellet).

Figure S27. IR spectra of $(PP^{Me}P)Ni(\eta^2-{}^{12}CO_2)$ (**3**, blue line) and $(PP^{Me}P)Ni(\eta^2-{}^{13}CO_2)$ (**3-${}^{13}CO_2$**, red line) (KBr pellet).
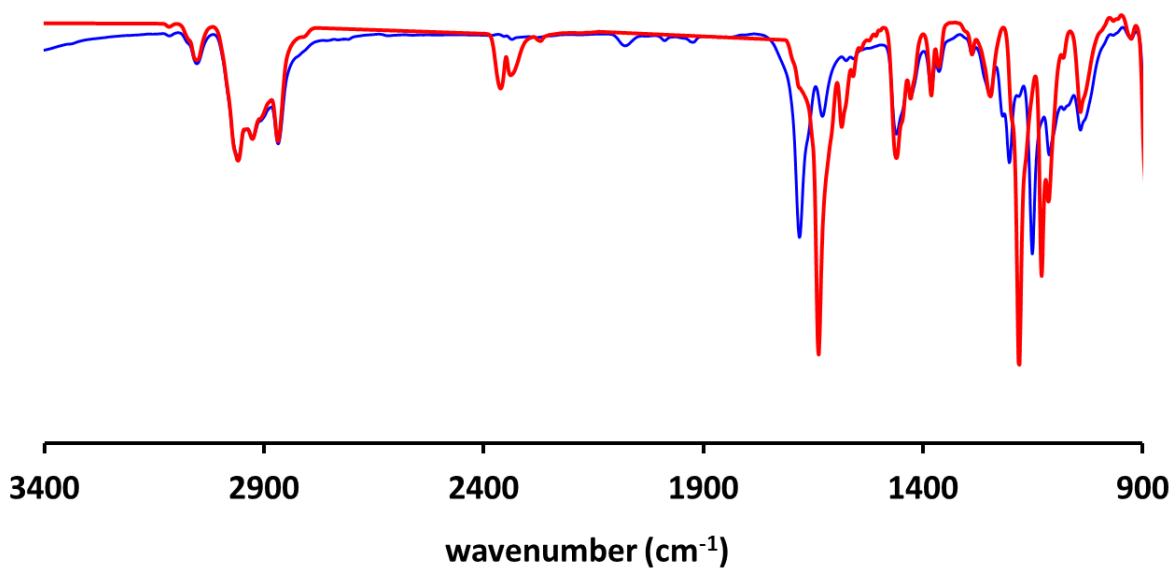
Figure S28. IR spectra of $(PP^{Me}P)Ni(\eta^2-CO_2)$ (**3**, dotted red line) and $(PP^{Me}P)Ni\{COOB(C_6F_5)_3\}$ (**4**, blue line) (KBr pellet).

23
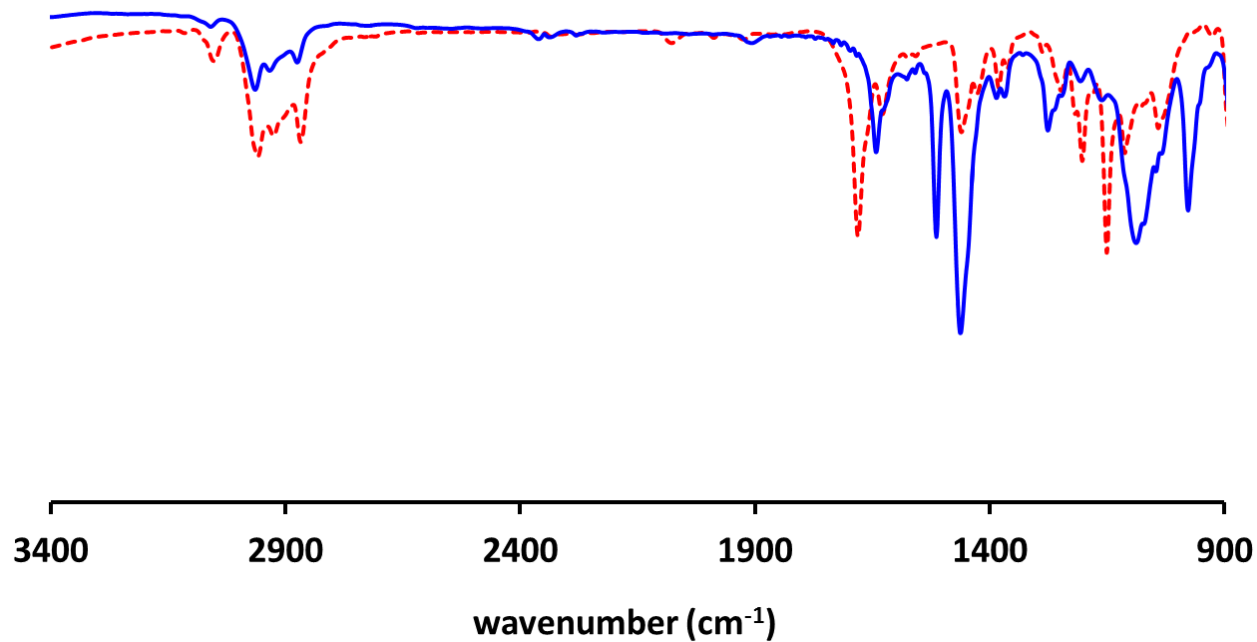
Figure S29. IR spectra of $(PP^{Me}P)Ni\{^{12}COOB(C_6F_5)_3\}$ (**4**, blue line) and $(PP^{Me}P)Ni\{^{13}COOB(C_6F_5)_3\}$ (**4-^{13}CO$_2$**, red line) (KBr pellet).
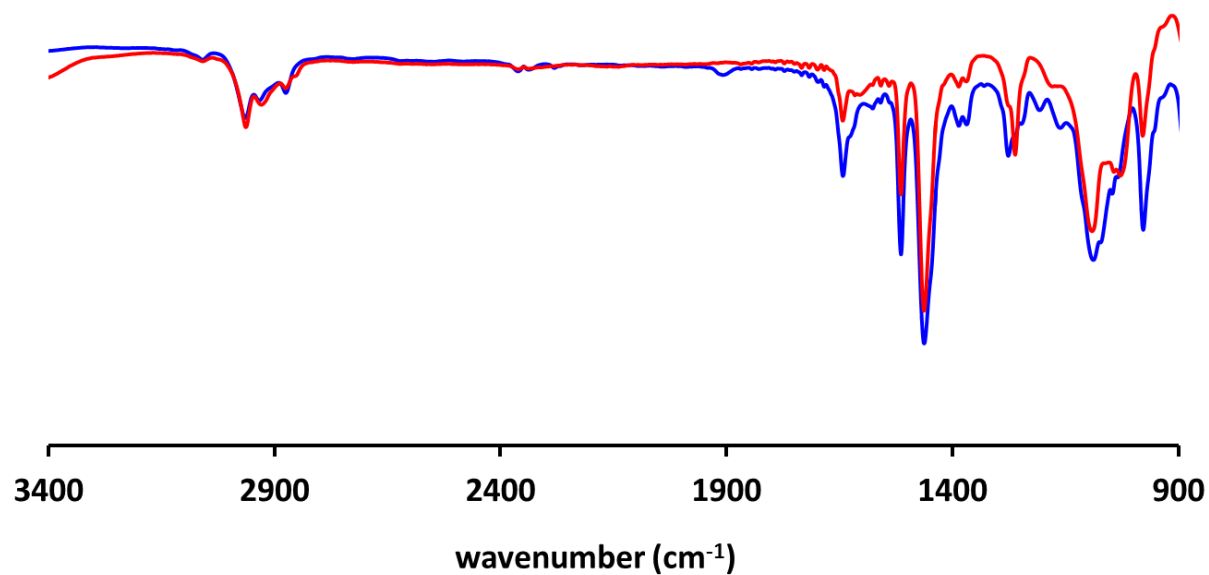
Figure S30. Raman spectra of $(PP^{Me}P)Ni(N_2)$ (**1**, green), $\{(PP^{Me}P)Ni\}_2(\mu\text{-}^{14}N_2)$ (**2**, red) and $\{(PP^{Me}P)Ni\}_2(\mu\text{-}^{15}N_2)$ (**2-^{15}N$_2$**, blue) in benzene at room temperature.
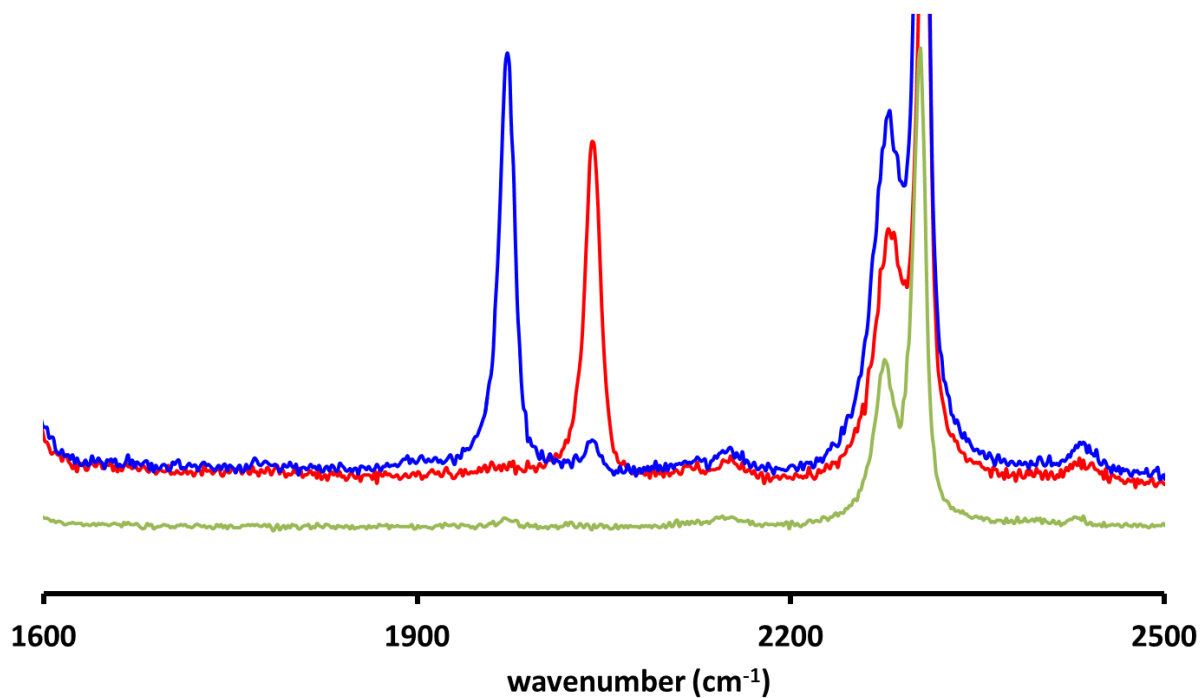
Figure S31. Raman spectrum of $\{(PP^{Me}P)Ni\}_2(\mu\text{-}N_2)$ (**2**) measured with a solid powder sample at room temperature.

25
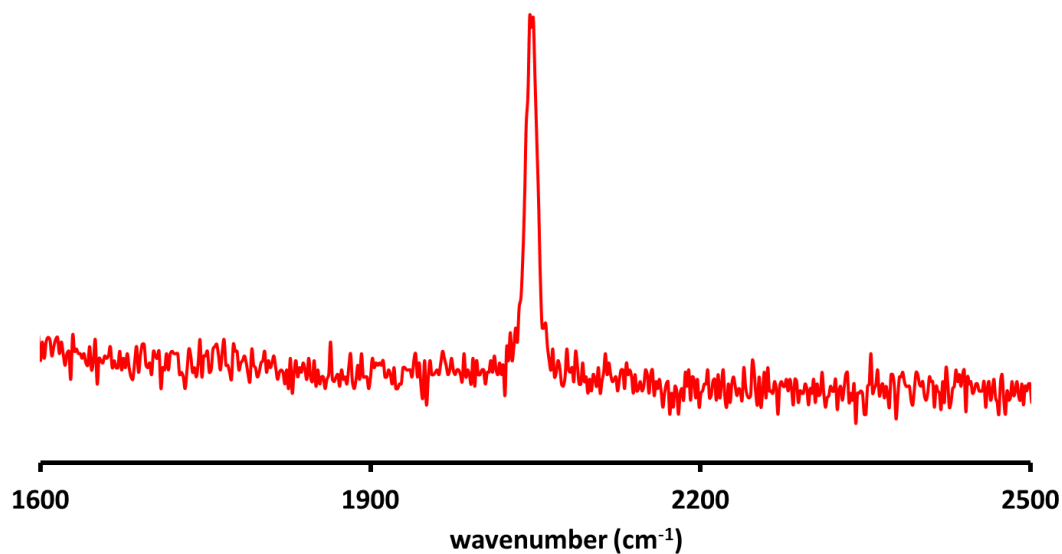
Figure S32. Solution IR spectra of $(PP^{Me}P)Ni(^{14}N_2)$ (**1**, red) and $(PP^{Me}P)Ni(^{15}N_2)$ (**1-^{15}N$_2$**, blue) in benzene-d_6 at room temperature (KBr window).
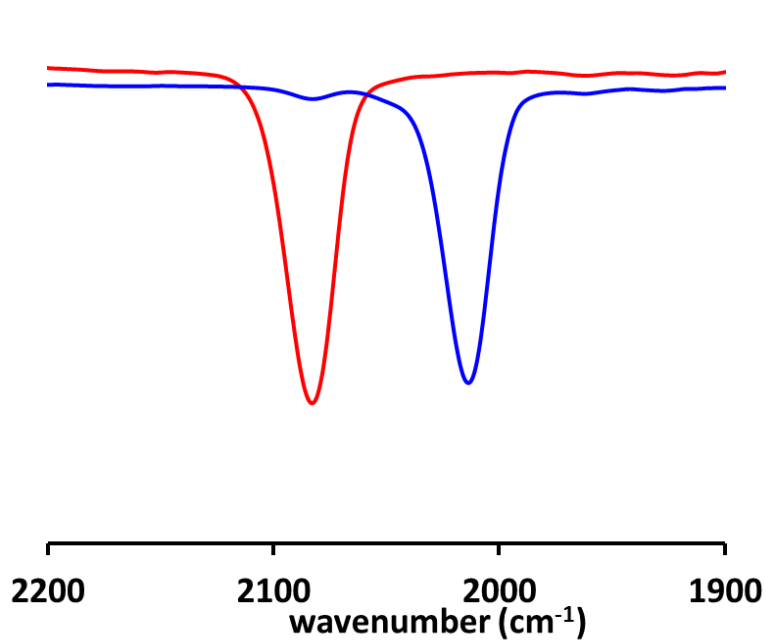
Figure S33. ESI mass data of $PP^{Me}P$; blue bars represent calculated values and red bars represent experiment values.
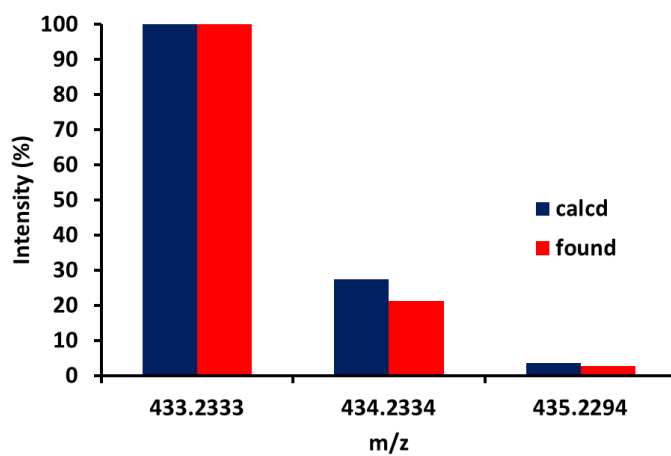
Figure S34. Electronic structures for (dtbpe)NiCO$_2$ and (PP^{Me}P)Ni(η^2-CO$_2$) (**3**) derived from the single point DFT calculations; energies in cm^{-1}.
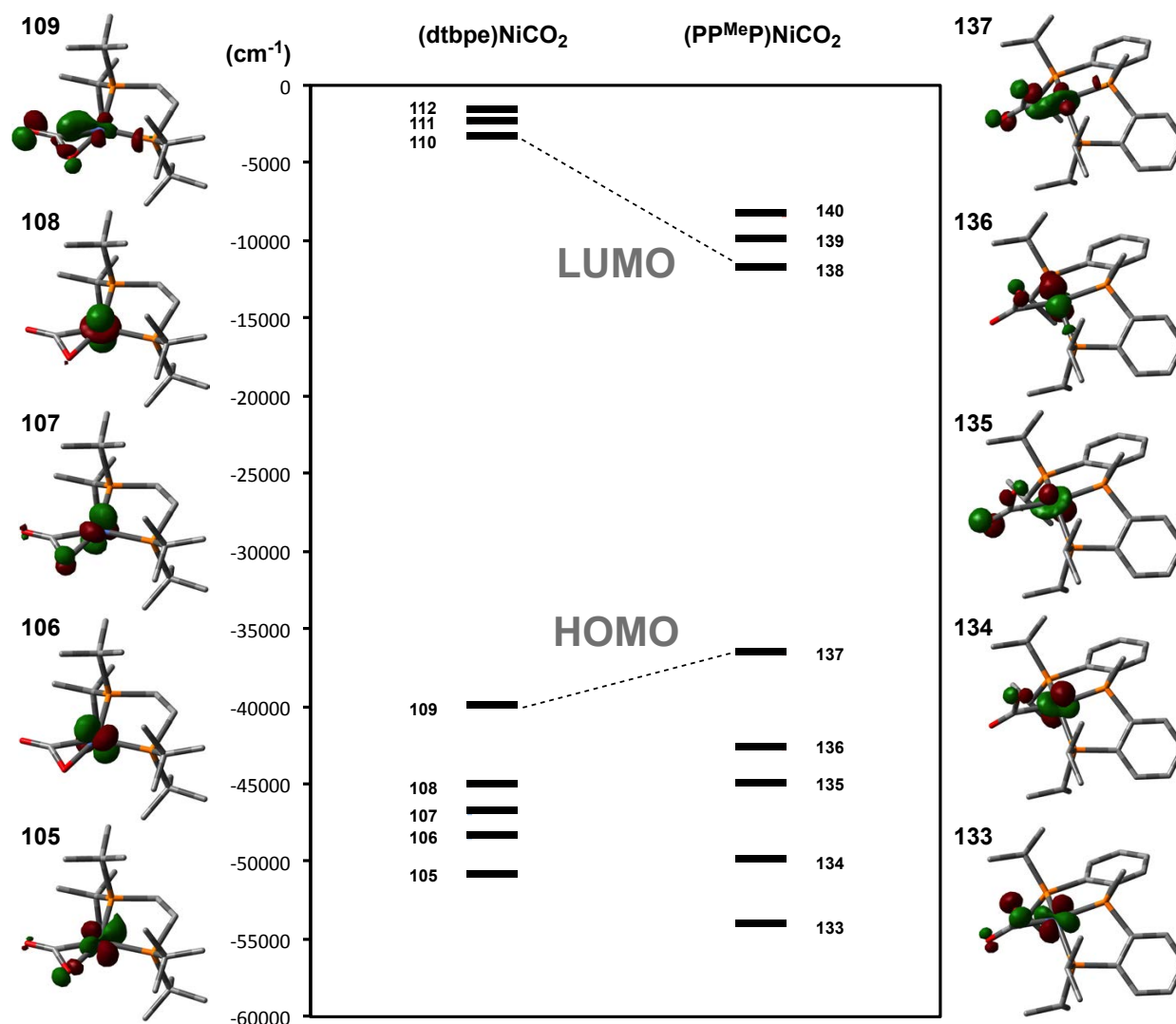
* Lobal representations correspond to the orbitals indicated by the number with 0.08 isocontours.

Figure S35. DFT calculated HOMOs for (dtbpe)NiCO$_2$ ((a) top view and (b) side view) and (PP^{Me}P)Ni(η^2-CO$_2$) (**3**, (c) top view and (d) side view).
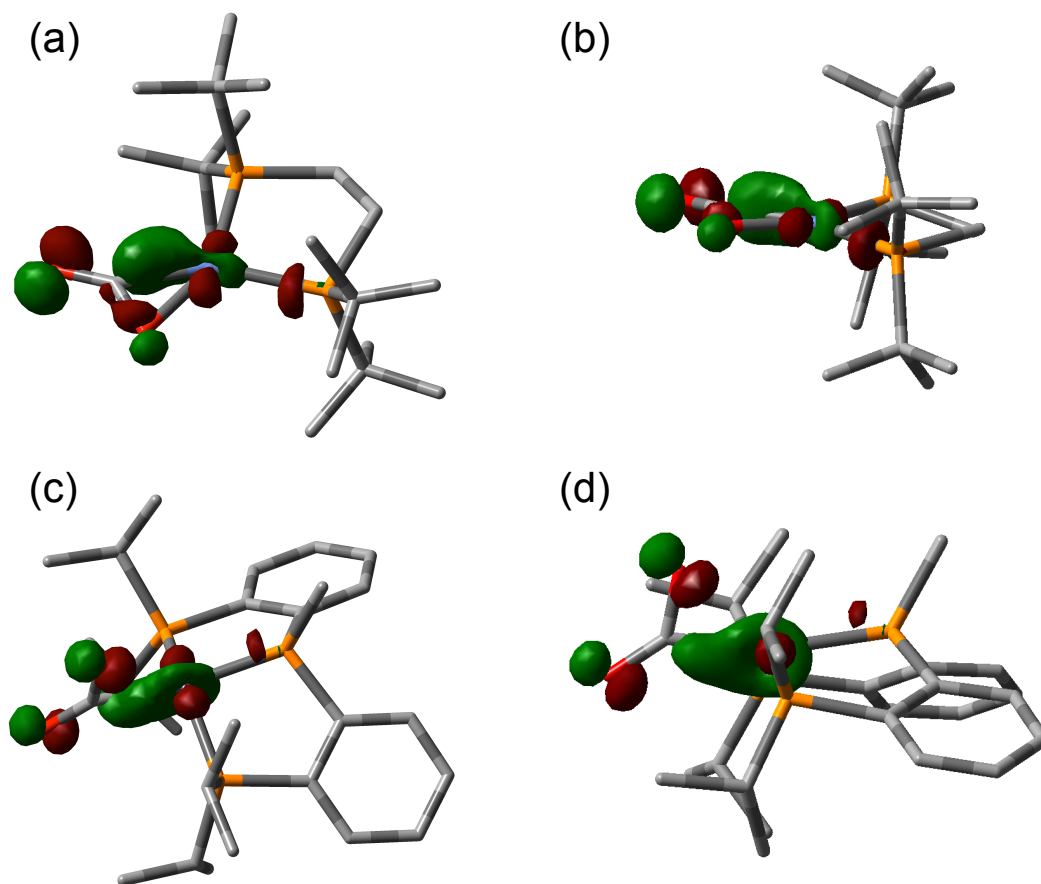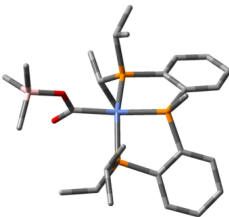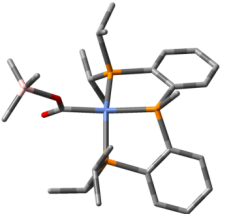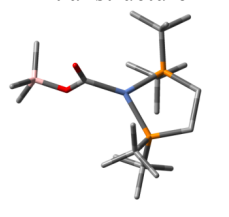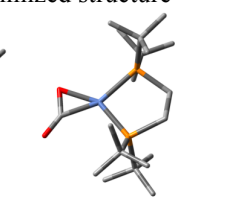
Figure S36. Electronic structures for $(PP^{Me}P)Ni\{COOB(CH_3)_3\}$ and $(dtbpe)NiCO_2-B(CH_3)_3$ derived from the single point DFT calculations; energies in cm^{-1}.
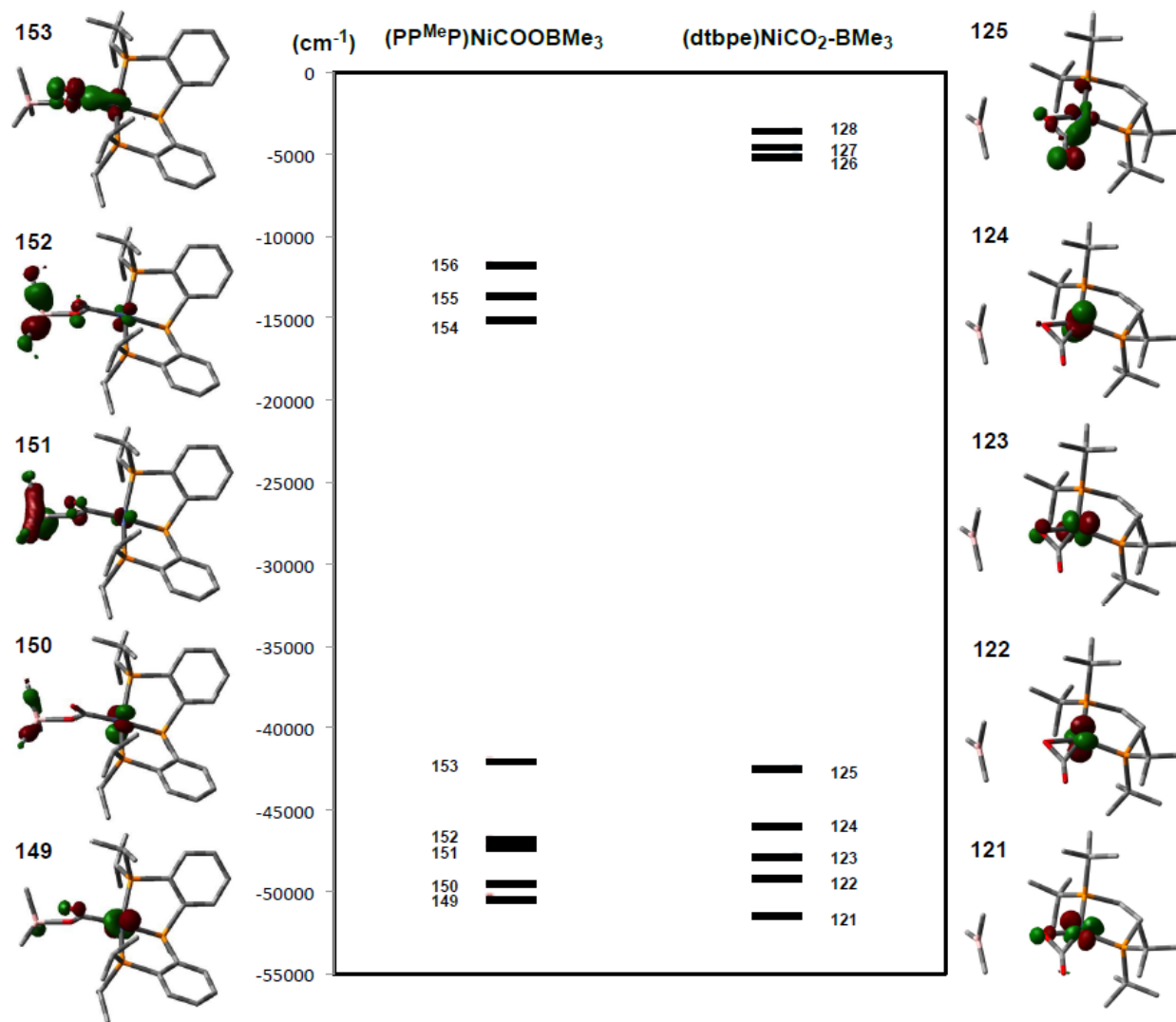
Lobal representations correspond to the orbitals indicated by the number with 0.08 isocontours.

Table S4. Selected bond distances and angles for $(PP^{Me}P)Ni\{COOB(CH_3)_3\}$ and $(dtbpe)NiCO_2$-$B(CH_3)_3$ from the single point DFT calculations (Å and °).

	$(PP^{Me}P)Ni\{COOB(CH_3)_3\}$		$(dtbpe)NiCO_2$-$B(CH_3)_3$	
	Initial structure[a]	Optimized structure[b]	Initial structure[c]	Optimized structure[b]
Ni-C	1.927	1.918	1.920	1.861
C=O	1.219	1.223	1.219	1.215
C-O	1.341	1.283	1.341	1.272
O-B	1.525	1.724	1.525	3.563
O-C-O	122.72	132.86	122.72	138.57

a. Entire coordinates were obtained from the compound **4** and further modified to replace all C_6F_5 groups with methyl groups.
b. Geometry optimizations were conducted with the corresponding initial structure.
c. Coordinates for a $(dtbpe)NiCO_2$ portion were obtained from the literature[6] and the same coordinates of BM_3 in $(PP^{Me}P)Ni\{COOB(CH_3)_3\}$ were used.

Table S5. Selected bond indices and bond orbital occupancies for $(dtbpe)Ni(\eta^2\text{-}CO_2)$ and $(PP^{Me}P)Ni(\eta^2\text{-}CO_2)$ (**3**) from NBO analysis.

	$(dtbpe)Ni(\eta^2\text{-}CO_2)$		$(PP^{Me}P)Ni(\eta^2\text{-}CO_2)$ (**3**)	
Wiberg Bond Index				
Ni-C	0.5766		0.5286	
Ni-O	0.4300		0.3117	
C=O	1.6927		1.6384	
C-O	1.4080		1.4701	
Bond Orbital Occupancy				
Ni-C	1.72868 (46.91% Ni, 53.09% C)		1.63916 (48.12% Ni, 51.88% C)	
Ni-O	1.71137 (1.78% Ni, 98.22% O)			
C=O	1.99612 (25.66% C, 74.34% O)		1.99296 (24.55% C, 75.45% O)	
C-O	1.99423 (69.53% O, 30.47% C)		1.96039 (66.31% O, 33.69% C)	
Ni (LP)	1.98794	1.91362	1.96870	1.91123
	1.93990	0.16087	1.95428	0.14993
	1.94327		1.91246	

Table S6. Selected bond indices and bond orbital occupancies for $(dtbpe)NiCO_2\text{-}B(CH_3)_3$ and $(PP^{Me}P)Ni\{COOB(CH_3)_3\}$ from NBO analysis.

	$(dtbpe)NiCO_2\text{-}B(CH_3)_3$		$(PP^{Me}P)Ni\{COOB(CH_3)_3\}$	
Wiberg Bond Index				
Ni-C	0.5830		0.5774	
Ni-O	0.3939		0.1552	
C=O	1.6728		1.6357	
C-O	1.4245		1.2764	
B-O	0.0028		0.4375	
Bond Orbital Occupancy				
Ni-C	1.72000 (53.70% C, 46.30% Ni)		1.65895 (40.51% Ni, 59.49% C)	
Ni-O	1.70874 (98.57% O, 1.43% Ni)			
B-O			1.91773 (86.63% O, 13.37% B)	
C=O	1.99544 (74.83% O, 25.17% C)		1.98465 (72.37% O, 27.63% C)	
	1.98724 (65.65% O, 34.35% C)		1.98246 (69.23% O, 30.77% C)	
C-O	1.99383 (69.47% O, 30.53 % C)		1.97766 (68.35% O, 31.65% C)	
Ni (LP)	1.98793	1.88315	1.97650	1.92248
	1.93944	0.14181	1.95525	0.08748
	1.94862		1.94779	

References

1. N. P. Mankad, E. Rivard, S. B. Harkins and J. C. Peters, *J. Am. Chem. Soc.,* 2005, **127**, 16032.

2. *SMART*, version 5.0; Data collection software; Bruker AXS, Inc.: Madison, WI, 1998

3. *SAINT*, version 5.0; Data integration software; Bruker AXS, Inc.: Madison, WI, 1998.

4. G. M. Sheldrick, SADABS: Program for absorption correction with the Bruker SMART system, Universitat Gottingen, Germany,1996.

5. Gaussian 09, Revision A.02, M. J. Frisch, G. W. Trucks, H. B. Schlegel, G. E. Scuseria, M. A. Robb, J. R. Cheeseman, G. Scalmani, V. Barone, B. Mennucci, G. A. Petersson, H. Nakatsuji, M. Caricato, X. Li, H. P. Hratchian, A. F. Izmaylov, J. Bloino, G. Zheng, J. L. Sonnenberg, M. Hada, M. Ehara, K. Toyota, R. Fukuda, J. Hasegawa, M. Ishida, T. Nakajima, Y. Honda, O. Kitao, H. Nakai, T. Vreven, J. A. Montgomery, Jr., J. E. Peralta, F. Ogliaro, M. Bearpark, J. J. Heyd, E. Brothers, K. N. Kudin, V. N. Staroverov, R. Kobayashi, J. Normand, K. Raghavachari, A. Rendell, J. C. Burant, S. S. Iyengar, J. Tomasi, M. Cossi, N. Rega, J. M. Millam, M. Klene, J. E. Knox, J. B. Cross, V. Bakken, C. Adamo, J. Jaramillo, R. Gomperts, R. E. Stratmann, O. Yazyev, A. J. Austin, R. Cammi, C. Pomelli, J. W. Ochterski, R. L. Martin, K. Morokuma, V. G. Zakrzewski, G. A. Voth, P. Salvador, J. J. Dannenberg, S. Dapprich, A. D. Daniels, Ö. Farkas, J. B. Foresman, J. V. Ortiz, J. Cioslowski, and D. J. Fox, Gaussian, Inc., Wallingford CT, **2009**.

6. J. S. Anderson, V. M. Iluc and G. L. Hillhouse, *Inorg Chem.*, 2010, **49**, 10203.

7. W. W. Weare, X. Dal, M. J. Byrnes, J. M. Chin, R. R. Schrock and P. Muller, *Proc. Natl. Acad. Sci.*, 2006, **103**, 17099.